
When Does A Spectral Graph Neural Network Fail in Node Classification?

Zhixian Chen¹ Tengfei Ma² Yang Wang¹

Abstract

Spectral Graph Neural Networks (GNNs) with various graph filters have received extensive affirmation due to their promising performance in graph learning problems. However, it is known that GNNs do not always perform well. Although graph filters provide theoretical foundations for model explanations, it is unclear when a spectral GNN will fail. In this paper, focusing on node classification problems, we conduct a theoretical analysis of spectral GNNs performance by investigating their prediction error. With the aid of graph indicators including homophily degree and response efficiency we proposed, we establish a comprehensive understanding of complex relationships between graph structure, node labels, and graph filters. We indicate that graph filters with low response efficiency on label difference are prone to fail. To enhance GNNs performance, we provide a provably better strategy for filter design from our theoretical analysis - using data-driven filter banks, and propose simple models for empirical validation. Experimental results show consistency with our theoretical results and support our strategy.

1. Introduction

Graph Neural Networks (GNNs) have continuously attracted interest as their promising performance in various graph learning problems. It is known that most of GNNs are intrinsically graph filters (Kipf & Welling, 2017; Defferrard et al., 2016; Ortega et al., 2018; Nt & Maehara, 2019). With the theoretical foundation of filters, there is an increasing attempt at model explanation, e.g. explaining the behavior of various GNNs in node classification. (Nt & Maehara, 2019) investigated the superiority of low-pass filters backed up with theoretical arguments while recent research (Balcilar et al., 2020; Chang et al., 2020; Bo et al., 2021) empirically revealed the weakness of GNNs with only low-pass filters in certain datasets. These contradictory views bring us to a question: why does a graph filter work on a dataset but not on another? More general, *when does a graph filter fail and what limits its prediction performance?*

Existing theoretical research is mostly restricted to the investigation of filters themselves, such as exploring their expressive power (Oono & Suzuki, 2020; Balcilar et al., 2020), without taking their inconsistency of performance on different graphs into account. In this paper, we conduct a theoretical analysis of spectral GNNs performance by investigating their prediction errors on different graphs. Our preliminary result of prediction error encourages us to have a comprehensive understanding of the complex and ambiguous relationships between graph structure, node labels, and graph filters. In Sect.4, we propose significant graph indicators including *interaction probability* (as a metric of homophily) and *response efficiency*. With the aid of them, we perform further analysis on prediction error which underpins deep insights of the failure of graph filters: 1. A graph filter fails when it has **low response efficiency** on label difference or input difference; 2. A graph filter is a hidden structure-adjustment mechanism and it fails when it is limited to make **graph homophilic high** enough by strengthening internal connections of classes; 3. Graph filters are prone to fail on graphs with **low information label differences**. It leads us to another question: *how to design filters to improve GNNs performance?*

To address this concern, we apply our theoretical results to typical graph filters and investigate their potential behavior on different graphs. We show that low-pass filters are superior to high-pass filters in homophilic graphs and high-order filters have an advantage over low order filters in most cases. In addition, we provide a theoretical demonstration of the **superiority of filter banks** which have only been empirically used in previous works to enhance GNNs performance (Min et al., 2020; Gao et al., 2021). Based on these explorations, we propose an effective strategy for filter design, that is, learning

¹Department of Mathematics, Hong Kong University of Science and Technology, Hong Kong SAR, China ²IBM T. J. Watson Research Center, New York, USA. Correspondence to: Zhixian Chen <zchenzc@connect.ust.hk>, Tengfei Ma <Tengfei.Ma1@ibm.com>.

filter banks in a data-driven manner.

To verify the effectiveness of the strategy we proposed, we develop a simple framework, named DEMUF, to learn data-specified filter banks efficiently and examine our models on various datasets. Experimental results show that our model achieves a significant performance improvement compared with spectral GNN baselines across most benchmarks and have strong consistency with our theoretical conclusions.

The rest of the paper is organized as follows: we formulate the prediction error of spectral GNNs and obtain a general lower bound in Sect.3. In Sect.4, we propose two groups of graph indicators which underpins our deep insights of graph filters from the spatial and spectral perspectives in Sect.5. Following that, we draw two main conclusions in Sect.5.1 and apply them to three types of filters in Sect.5.2. In Sect.6, we develop a simple framework to implement the strategy we proposed for filter design and empirically validate our theoretical analysis.

2. Related Work

In this paper, we focus on the analysis of the performance of GNNs from the spectral perspective. Since Bruna et al. (2014) defined spectral graph filters and extended convolutional operations to graphs, various spectral graph neural networks have been developed. For example, ChebNet (Defferrard et al., 2016) defines the Chebyshev polynomial filter which can be exactly localized in the k-hop neighborhood. Kipf & Welling (2017) simplified the Chebyshev filters using a first-order approximation and derived the well-known graph convolutional networks (GCNs). Bianchi et al. (2021) proposed the rational auto-regressive moving average graph filters (ARMA) which are more powerful in modeling the localization and provide more flexible graph frequency response, however more computationally expensive and also more unstable. Recently, Min et al. (2020) augmented conventional GCNs with geometric scattering transforms which enabled second-order filtering of graph signals and alleviated the over-smoothing issue. In addition, most graph neural networks originally defined in the spatial domain are also found essentially connected to the spectral filtering (Balcilar et al., 2020). By bridging the gap between spatial and spectral graph neural networks, Balcilar et al. (2020) further investigated the expressiveness of all graph neural networks from their spectral analysis. However, their analysis is limited to the spectrum coverage of a graph filter itself and lacks deeper insights into the graph-dependent performance of these filters.

Another related topic is the graph homophily/heterophily. One important graph indicator we propose in the paper is the homophily degree which we define through the interaction probability. Beyond that, there have been some other heuristic metrics for homophily/heterophily in previous works. Pei et al. (2020) defined a node homophily index to characterize their datasets and help explain their experimental results for Geom.GCN. Zhu et al. (2020) defined edge homophily ratio instead and identified a set of key designs that can boost learning from the graph structure in heterophily. Some recent works analyzed the impact of heterophily on the performance of GNNs (Zhu et al., 2020; Jin et al., 2021; Ma et al., 2021), but they are either limited to empirical study (Zhu et al., 2020; Jin et al., 2021) or just focused on GCNs (Ma et al., 2021). Our work differs from these works in that our homophily degree definition is only used as one of the graph indicators in our theoretical analysis of GNNs performance, and our analysis is also not limited to GCNs but for all spectral GNNs.

3. Theoretical Analysis of Prediction Error

3.1. Problem Formulation

Notations. Let \mathcal{G}_n be an undirected graph with additional self-connection, $A \in \mathbb{R}^{n \times n}$ be the adjacency matrix and $L = D - A$ be the Laplacian matrix, where D is a diagonal degree matrix with $D_{ii} = \sum_j A_{ij}$. We denote $\tilde{A} = D^{-\frac{1}{2}} A D^{-\frac{1}{2}}$ and $\tilde{L} = I - \tilde{A}$ as the symmetric normalized Laplacian. Let $(\lambda_i, \mathbf{u}_i)$ be a pair of eigenvalue and unit eigenvector of \tilde{L} , where $0 = \lambda_0 \leq \dots \leq \lambda_{n-1} \leq 2$. In graph signal processing (GSP), $\{\lambda_i\}$ and $\{\mathbf{u}_i\}$ are called frequencies and frequency components of graph \mathcal{G}_n .

In this paper, we are mainly interested in multi-class node classification problems on \mathcal{G}_n with labels $\mathcal{T} = \{0, \dots, K - 1\}$. For $\forall k \in \mathcal{T}$, we denote \mathcal{C}_k as the set of nodes with label k and introduce a label matrix $Y \in \mathbb{R}^{n \times K} = (\mathbf{y}_0, \dots, \mathbf{y}_{K-1})$, where \mathbf{y}_k is the indicator vector of \mathcal{C}_k . Let $R = Y^\top Y$, then $Y^\top \mathbb{1} = \text{diag}(R)$ and $R_k = |\mathcal{C}_k|$. The general formulation of the $l + 1$ -th layer of spectral GNNs is $X^{(l+1)} = \sigma(g(\tilde{L})X^{(l)}W^{(l+1)})$, here $g(\tilde{L})$ is so-called the graph filter, $\sigma(\cdot)$ is an activation function and $W^{(l+1)}$ is a learnable matrix. In multi-class classification problems, $\sigma(\cdot) = \text{softmax}(\cdot)$. In this paper, we say $X^{(l)}W^{(l+1)}$ is the input of $g(\tilde{L})$ in $l + 1$ -th layer.

3.2. Prediction Error

Definition 3.1 (Prediction error). For a graph \mathcal{G}_n with \tilde{L} , let $X = (\mathbf{x}_0, \dots, \mathbf{x}_{K-1})$ be the learnable input of $g(\tilde{L})$ in the last layer and $Y = (\mathbf{y}_0, \dots, \mathbf{y}_{K-1})$ be the label matrix, the prediction error is formulated as:

$$Er(X, Y) = \|\sigma(g(\tilde{L})X) - Y\|_F^2 = \sum_{l \in \mathcal{T}} Er(\mathbf{x}_l, \mathbf{y}_l), \quad (1)$$

$$Er(\mathbf{x}_l, \mathbf{y}_l) = \left\| \frac{e^{g(\tilde{L})\mathbf{x}_l}}{e^{g(\tilde{L})\mathbf{x}_l} + \sum_{k \neq l} e^{g(\tilde{L})\mathbf{x}_k}} - \mathbf{y}_l \right\|_2^2. \quad (2)$$

Since $Er(X, Y) = \sum_{l \in \mathcal{T}} Er(\mathbf{x}_l, \mathbf{y}_l)$, estimating the entire prediction error equals to estimate that of any single label. Without loss of generality, in the following discussion, we focus on label \mathbf{y}_0 and investigate $Er(\mathbf{x}_0, \mathbf{y}_0)$. By denoting $\mathbf{y}'_0 = \mathbf{y}_0$ and $\mathbf{y}'_1 = \sum_{l=1}^{K-1} \mathbf{y}_l$, we obtain a corresponding binary classification problem where $Er(\mathbf{x}'_0, \mathbf{y}'_0)$ is an approximation of $Er(\mathbf{x}_0, \mathbf{y}_0)$. For simplicity, in the rest of paper, we investigate $Er(\mathbf{x}_0, \mathbf{y}_0)$ in a binary classification. The theorem below provides a lower bound of it.

Theorem 3.2 (Prediction error). *In a binary classification problem with label matrix $Y = (\mathbf{y}_0, \mathbf{y}_1)$. Let $X = (\mathbf{x}_0, \mathbf{x}_1)$ be the input matrix, we have:*

$$\begin{aligned} Er(\mathbf{x}_0, \mathbf{y}_0) &\geq \frac{n}{4} - \frac{(\mathbf{y}_1 - \mathbf{y}_0)^\top \psi(\mathbf{z})}{4} + \frac{\|\psi(\mathbf{z})\|_2^2}{16} \\ &\quad - \frac{\|\psi(\mathbf{z})\|_3^3}{48} - \frac{\|\psi(\mathbf{z})\|_4^4}{96} - \frac{C}{(1+e)^2} \\ &> \frac{167}{800}n - \frac{1}{4} \sum_i \psi((\mathbf{y}_{1i} - \mathbf{y}_{0i})\mathbf{z}_i) \end{aligned}$$

where $\mathbf{z} = g(\tilde{L})(\mathbf{x}_1 - \mathbf{x}_0)$, $\psi(x) = \min\{\max\{x, -1\}, 1\}$ is a clamp function limiting x to $[-1, 1]$ and C is cardinality of $\mathcal{S}_{\mathbf{y}, \mathbf{z}} = \{(\mathbf{y}_{0i}, \mathbf{z}_i) | \mathbf{z}_i < -1, \mathbf{y}_{0i} = 1 \text{ or } \mathbf{z}_i > 1, \mathbf{y}_{0i} = 0\}$, i.e., $C = |\mathcal{S}_{\mathbf{y}, \mathbf{z}}|$.

The proof is in Appendix B.1. The first inequality holds when $\mathbf{x}_0 = \mathbf{x}_1$ where $Er(\mathbf{x}_0, \mathbf{y}_0) = \frac{n}{4}$. This theorem indicates that prediction errors of binary classification are dependent on graph filter $g(\tilde{L})$, $\Delta \mathbf{y} = \mathbf{y}_0 - \mathbf{y}_1$ and $\Delta \mathbf{x} = \mathbf{x}_0 - \mathbf{x}_1$, what we refer to as *label difference* and *input difference* in this paper, respectively. Then we have

$$Er(\mathbf{x}_0, \mathbf{y}_0) > \frac{167}{800}n - \frac{1}{4} \sum_i \psi(\Delta \mathbf{y}_i (g(\tilde{L}) \Delta \mathbf{x})_i). \quad (3)$$

It makes us aware of the need to fully understand their impact on the performance of spectral GNNs.

4. Proposed Graph Indicators

In this section, we explore the relationships between graph structure, graph signals including node labels, and graph filters and define related graph indicators which underpins our further investigation on prediction error in Sect.5.

4.1. Spatial Graph Indicators

Homophily of graphs is considered an indisputable common property of most graphs. In this section, we derive a measure of homophily degree from interaction probability.

For a random walk on \mathcal{G}_n , $P^k = (D^{-1}A)^k$ is the k -step transition matrix where P_{ij}^k is the probability that a random walker starting from node v_i arrives at v_j after k steps. $\sum_{j \in \mathcal{C}_l} P_{ij}^k$ is the probability that a random walker starting from v_i stays in \mathcal{C}_l at the k -th step, demonstrating the relative preference/closeness of node v_i for \mathcal{C}_l at k -th scale. Based on this, we define interaction probability to reflect the strength of interaction between two classes.

Definition 4.1 (k -step interaction probability). For $l, m \in \mathcal{T}$, denote $P^k = (D^{-1}A)^k$, the k -step interaction probability

matrix is formulated as:

$$\Pi_{lm}^k = \frac{1}{R_l} \sum_{v_i \in \mathcal{C}_l, v_j \in \mathcal{C}_m} P_{ij}^k = \frac{\mathbf{y}_l^\top P^k \mathbf{y}_m}{\mathbf{y}_l^\top \mathbf{y}_l} \quad (4)$$

$$\Pi^k = (Y^\top Y)^{-1} Y^\top P^k Y = R^{-1} Y^\top P^k Y. \quad (5)$$

Π_{lm}^k is the probability that a random walker from \mathcal{C}_l arrives at \mathcal{C}_m after k steps and $\sum_{m \in \mathcal{T}} \Pi_{lm}^k = 1$.

Since P is not symmetric, then $\Pi_{lm}^k \neq \Pi_{ml}^k$. Below we propose a *symmetric variant of interaction probability*, which plays a key role in our theoretical analysis.

Definition 4.2 (*k*-step symmetric interaction probability). For $l, m \in \mathcal{T}$, denote $\tilde{A}^k = (D^{-\frac{1}{2}} A D^{-\frac{1}{2}})^k$, the *k*-step symmetric interaction probability matrix is formulated as:

$$\tilde{\Pi}^k = R^{-\frac{1}{2}} Y^\top \tilde{A}^k Y R^{-\frac{1}{2}}. \quad (6)$$

Remark 4.3. If $|\mathcal{T}| \neq n$, $(R^{-\frac{1}{2}} Y^\top \tilde{A} Y R^{-\frac{1}{2}})^k \neq R^{-\frac{1}{2}} Y^\top \tilde{A}^k Y R^{-\frac{1}{2}}$, i.e. $(\tilde{\Pi})^k \neq \tilde{\Pi}^k$. Also, $(\Pi)^k \neq \Pi^k$. That is, *k*-step (symmetric) interaction probability is not the *k*-th power of 1-step (symmetric) interaction probability.

Notations. In the rest of paper, we take $\tilde{\pi}_l^k$ as the shorthand for $\tilde{\Pi}_{ll}^k$. We denote $\tilde{g}(\tilde{\Pi}) = R^{-\frac{1}{2}} Y^\top g(\tilde{A}) Y R^{-\frac{1}{2}}$ to avoid confusion with $g(\tilde{\Pi}) = g(R^{-\frac{1}{2}} Y^\top \tilde{A} Y R^{-\frac{1}{2}})$.

Noting that $\tilde{\Pi}^k \mathbf{1} \neq \mathbf{1}$, $\tilde{\Pi}^k$ is not a probability measure in the strict sense. However, it is a bridge to other graph indicators, as we will show in the rest of this section. Below, we show the relationship between $\tilde{\Pi}^k$ and Π^k .

Proposition 4.4 (Interaction probability). For $l, m \in \mathcal{T}$, $\tilde{\pi}_l^{2k} \geq (\tilde{\pi}_l^k)^2$ and $\pi_l^k \geq \tilde{\pi}_l^k$. More generally, $R_l \Pi_{lm}^k + R_m \Pi_{ml}^k \geq 2\sqrt{R_l R_m} \tilde{\Pi}_{lm}^k$.

The proof can be found in Appendix B.2. It indicates that $\tilde{\pi}_l^k$ is the lower bound of π_l^k . Recall the descriptive definition of graph homophily - nodes with the same labels are more likely to cluster together, for a homophilic graph with symmetric interaction probability $\tilde{\Pi}$, self-interaction probability $\tilde{\pi}_l^k$ is expected to gap away from $\{\tilde{\Pi}_{lm}^k | m \in \mathcal{T}, m \neq l\}$.

Definition 4.5 (*k*-homophily degree). For a graph \mathcal{G}_n with symmetric interaction probability $\tilde{\Pi}$, the *k*-homophily degree of \mathcal{G}_n is defined as

$$\begin{aligned} \mathcal{H}_k(\tilde{\Pi}|\mathcal{C}_l) &= \sqrt{\frac{R_l}{n}} \tilde{\pi}_l^k - \sum_{m \neq l} \sqrt{\frac{R_m}{n}} \tilde{\Pi}_{lm}^k, \\ \mathcal{H}_k(\tilde{\Pi}|\mathcal{G}_n) &= \sum_l \sqrt{\frac{R_l}{n}} \mathcal{H}_k(\tilde{\Pi}^k|\mathcal{C}_l) = \frac{1}{n} \sum_l (R_l \tilde{\pi}_l^k - \sum_{m \neq l} \sqrt{R_m R_l} \tilde{\Pi}_{lm}^k), \end{aligned} \quad (7)$$

where $\mathcal{H}_k(\tilde{\Pi}|\mathcal{C}_l)$ is the *k*-homophily degree of \mathcal{C}_l .

Remark 4.6. $\mathcal{H}_k(\tilde{\Pi}|\mathcal{C}_l), \mathcal{H}_k(\tilde{\Pi}|\mathcal{G}_n) \in [-1, 1]$. We say \mathcal{G}_n is a *k*-homophilic graph if $\mathcal{H}_k(\tilde{\Pi}|\mathcal{G}_n) > 0$.

In binary classification problems, $\mathcal{H}_k(\tilde{\Pi}|\mathcal{G}_n) = \frac{1}{n} (R_0 \tilde{\pi}_0^k + R_1 \tilde{\pi}_1^k - 2\sqrt{R_0 R_1} \tilde{\Pi}_{01}^k)$. Larger $\mathcal{H}_k(\tilde{\Pi}|\mathcal{C}_l)$ means \mathcal{C}_l have denser internal connections and sparser connections between other classes. Then intuitively, $\mathcal{H}_k(\tilde{\Pi}|\mathcal{G}_n)$ reflects the possibility to obtain a node's label directly from its neighbors. As we illustrate in Sect.5.1.2, one of the keys to the success of graph filters is to increase the possibility by strengthening internal connections of classes, that is, make graph more homophilic.

4.2. Spectral Graph Indicators

In this section, we develop another indicator - *repsonse efficiency*, to measure the effect of graph filters $g(\tilde{L})$ applied to different graph signals. Recall that $\{\lambda_i\}$ and $\{\mathbf{u}_i\}$ are graph frequencies and frequency components. For a graph signal \mathbf{x} with spectrum $\alpha = \{\alpha_i = \langle \mathbf{u}_i, \mathbf{x} \rangle\}$, we are able to represent it as $\mathbf{x} = \sum \alpha_i \mathbf{u}_i$. Noting that $\alpha_k^2 / \sum_i \alpha_i^2$ shows the percentage of occurrences in \mathbf{x} for each \mathbf{u}_k , we introduce a distributional representation of \mathbf{x} .

Definition 4.7 (Frequency distribution). We define \mathbf{f} , the frequency of signal \mathbf{x} , as a random variable taking values in the set of graph frequencies with probability $\Pr(\mathbf{f} = \lambda_k) = \alpha_k^2 / \sum_i \alpha_i^2$. The probability describes the frequency distribution of signal \mathbf{x} .

Since probability $\Pr(\mathbf{f} = \lambda_k) = \alpha_k^2 / \sum_i \alpha_i^2$ is the weight of \mathbf{u}_k in \mathbf{x} and $g(\lambda_k)$ reflects how filter $g(\tilde{L})$ acts on \mathbf{u}_k , then we claim that $\sum_k g(\lambda_k) \Pr(\mathbf{f} = \lambda_k)$ is the effect of $g(\tilde{L})$ acting on \mathbf{x} . Although an all-pass filter can pass all frequencies, we appreciate a filter with a high magnitude response for important frequencies so that we can capture the main frequency information of a signal \mathbf{x} efficiently.

Definition 4.8 (Response Efficiency). For a graph filter $g(\tilde{L})$ and a signal \mathbf{x} with spectrum α , the response efficiency of $g(\tilde{L})$ on \mathbf{x} is defined as

$$\mu_g(\mathbf{x}) = \frac{\sum_i g(\lambda_i) \alpha_i^2}{\left(\sum_i g(\lambda_i)\right) \left(\sum_i \alpha_i^2\right)}.$$

It can also be denoted as $\mu_g(\alpha)$.

We obtain a high response efficiency when the magnitude response of $g(\tilde{L})$ is positively associated with the frequency distribution of \mathbf{x} . In Sect.5.1.1, we have further discussion of the relationship between graph response efficiency and its prediction performance. Before that, we investigate the consistency of proposed graph indicators.

Proposition 4.9. Let \mathbf{f}_l be the frequency of label \mathbf{y}_l , for a graph filter $g(\cdot)$, we have $\mu_g(\mathbf{y}_l) = \frac{(\tilde{g}(I - \tilde{\Pi}))_{ll}}{\sum_i g(\lambda_i)}$. Specially, when $g = (\cdot)^n$, $\mu_g(\mathbf{y}_l) = \frac{\mathbb{E}[\mathbf{f}_l^n]}{\sum_i g(\lambda_i)}$.

The proof of this proposition can be found in Appendix B.2. Recall that $\tilde{g}(I - \tilde{\Pi}) = R^{-\frac{1}{2}} Y^\top g(I - \tilde{A}) Y R^{-\frac{1}{2}}$, we have $\mathbb{E}[\mathbf{f}_l] = 1 - \tilde{\pi}_l$, $\mathbb{E}[\mathbf{f}_l^2] = 1 - 2\tilde{\pi}_l + \tilde{\pi}_l^2$ and the variance of \mathbf{f}_l : $\text{Var}(\mathbf{f}_l) = \tilde{\pi}_l^2 - (\tilde{\pi}_l)^2$. According to Proposition 4.4, $\tilde{\pi}_l \leq \pi_l \leq 1$ and $\tilde{\pi}_l^2 \geq (\tilde{\pi}_l)^2$. Therefore, when $\tilde{\pi}_l$ approaches 1, which reflects a high homophily degree of \mathcal{C}_l , both the mean and variance of label frequency are close to 0. It implies that, **for a highly homophilic graph, the main information of labels is low-frequency so it should be assigned to low-pass filters**. Rigorous support for this argument can be found in Sect.5.2.

5. Analysis of Graph Filters

In this section, we aim to figure out two major concerns: *what causes the failure of a graph filter and how to design filters to improve GNNs performance?* Precisely, we first provide a deep understanding of the performance of graph filters concerning label prediction with the aid of graph indicators we proposed above, then apply our theoretical conclusion to typical filters. From this, we have obtained insights into filter design.

5.1. Analysis of Prediction Error

In this section, we focus on a family of polynomial filters $\mathcal{S}_g = \{g \text{ is polynomial } | g([0, 2]) \in [0, 1], \sum_i g(\lambda_i) > 1\}$. We denote $\mathcal{I}_g = \{i | g(\lambda_i) \neq 0, i = 0, \dots, n-1\}$ as the indicator set of nonzero elements in $\{g(\lambda_i)\}$.

5.1.1. FROM FILTER RESPONSE EFFICIENCY

Let δ, η be the spectra of $\Delta \mathbf{y}$, $\Delta \mathbf{x}$, respectively, it is trivial to revisit the inequality (3) of $Er(\mathbf{x}_0, \mathbf{y}_0)$ as:

$$Er(\mathbf{x}_0, \mathbf{y}_0) > \frac{167}{800} n - \frac{1}{4} \sum_i \psi(g(\lambda_i) \delta_i \eta_i).$$

We attempt to establish an analysis of $\sum_i \psi(g(\lambda_i) \delta_i \eta_i)$ which is the critical term of this lower bound in the spectral domain. Before that, we introduce information content proposed by information theory to measure the informativeness of signal frequency.

Definition 5.1 (Information content). For a signal with spectrum δ , we say $\mathbf{I}(\delta) = - \sum_{i \in \mathcal{I}_\delta} \log \frac{\delta_i^2}{\sum_k \delta_k^2}$ is the information content of δ where $\mathcal{I}_\delta = \{i | \delta_i \neq 0, i = 0, \dots, n-1\}$ is the indicator set of nonzero elements of δ .

Theorem 5.2. Given a label difference $\Delta \mathbf{y}$ with spectrum δ , for an arbitrary input difference $\Delta \mathbf{x}$ with spectrum η , for a graph filter $g(\cdot) \in \mathcal{S}_g$, we construct $\tilde{\eta}_i = \psi_{\frac{1}{g(\lambda_i) \delta_i}}(\eta_i)$, where $\psi_{\frac{1}{g(\lambda_i) \delta_i}}(x) = \min\{\max\{x, -\frac{1}{g(\lambda_i) \delta_i}\}, \frac{1}{g(\lambda_i) \delta_i}\}$ is a clamp function such that $|\tilde{\eta}_i g(\lambda_i) \delta_i| \leq 1$ and

$$\sum_{i=0}^{n-1} \psi(\eta_i g(\lambda_i) \delta_i) \leq \frac{1}{m_g} \min\{\mathcal{M}(g, \delta), \mathcal{M}(g, \tilde{\eta})\}, \quad (8)$$

where $m_g = \min_{i \in \mathcal{I}_{g,\delta,\tilde{\eta}}} g(\lambda_i)$, $c(g, \delta) = \frac{\sum_{i \in \mathcal{I}_{g-\mathcal{I}_{g,\delta}} g(\lambda_i)} g(\lambda_i)}{\sum_{i \in \mathcal{I}_{g,\delta}} g(\lambda_i)}$ and $\mathcal{M}(g, \delta) = \frac{-\mathbf{I}(\delta)}{\log(1+c(g,\delta))\mu_g(\delta)}$ with $\mathcal{I}_{g,\delta} = \mathcal{I}_g \cap \mathcal{I}_\delta$.

The theorem indicates that the **prediction error of a given graph filter is bounded by its response efficiency on labels and inputs difference**. In GNNs, inputs are learnable. Ideally, a GNN with filter g can learn appropriate inputs with large enough $\mu_g(\eta)$. In this way, the prediction error will be restricted only by the graph structure, node labels, and the filter itself, that is what Corollary 5.3 illustrates.

Corollary 5.3 (Spectral lower bound). *For a binary classification problem, with the same settings and notations in Theorem 5.2, we have*

$$Er(\mathbf{x}_0, \mathbf{y}_0) > \frac{167}{800}n + \frac{\mathbf{I}(\delta)}{m_g \log(1+c(g,\delta))\mu_g(\delta)} \quad (9)$$

For a given classification problem, we claim that a graph filter fails if the lower bound of its prediction error is large. Corollary 5.3 (proof is provided in Appendix B.5) impels us toward deep insights of graph filters in terms of response efficiency: 1. **A graph filter fails when it has low response efficiency on label difference**, i.e., small $\mu_g(\delta)$, which means that it can't capture the main information used for label identification efficiently; 2. **Most filters fail on graphs with low information label difference**, i.e., small $\mathbf{I}(\delta)$, which means that a closed difference of labels' probability on different frequency components would have been difficult to distinguish.

5.1.2. FROM GRAPH HOMOPHILY DEGREE

Recall the attempt we made to explore the relation between filter response efficiency on labels and graph homophily degree at the end of Sect.4, it inspires us to explain graph filters from a perspective of graph homophily.

Theorem 5.4 (Spatial lower bound). *Given a binary classification problem on a graph \mathcal{G}_n whose label difference is Δy with spectrum δ , for a graph filter $g(\cdot) \in \mathcal{S}_g$ and arbitrary input X , we have*

$$Er(X, Y) > \frac{167}{400}n + \frac{\mathbf{I}(\delta)}{2m_g \log \frac{\mathcal{H}_1(\tilde{g}(I - \tilde{\Pi})|\mathcal{G}_n)}{\sum_i g(\lambda_i)}}, \quad (10)$$

where $m_g = \min_{i \in \mathcal{I}_{g,\delta}} g(\lambda_i)$, $\tilde{g}(I - \tilde{\Pi}) = R^{-\frac{1}{2}}Y^\top g(I - \tilde{A})Y R^{-\frac{1}{2}}$ and $\mathcal{H}_1(\tilde{g}(I - \tilde{\Pi})|\mathcal{G}_n) = \frac{R_0}{n}(\tilde{g}(I - \tilde{\Pi}))_{00} + \frac{R_1}{n}\tilde{g}(I - \tilde{\Pi})_{11} - 2\frac{\sqrt{R_0 R_1}}{n}\tilde{g}(I - \tilde{\Pi})_{01}$.

The proof of Theorem 5.4 provided in Appendix B shows that for any function $g(\cdot)$ which is nonnegative on the closed interval $[0, 2]$, $\mathcal{H}_1(\tilde{g}(I - \tilde{\Pi})|\mathcal{G}_n) \in [0, 1]$.

This theorem brings us an explanation of graph filters in terms of homophily: *a graph filter is a hidden structure-adjustment mechanism* which transforms graph structure to $g(I - \tilde{A})$. It obtains poor prediction performance when it **fails to make the high homophily degree $\mathcal{H}_1(\tilde{g}(I - \tilde{\Pi})|\mathcal{G}_n)$ of transformed graph high enough**. From this, we are able to glimpse the prediction capacity of filters on a given graph through the modified homophily degree.

5.2. Applied to Specific Graph Filters

In this section, we apply the above observations to specific graph filters and provide practical strategies to enhance GNNs performance. Here, we consider typical filters including first/second-order low/high-pass filters and investigate their advantage/disadvantage on different graphs by comparing their $\mathcal{H}_1(\tilde{g}(I - \tilde{\Pi})|\mathcal{G}_n)$.

Notations. We denote $\mathcal{S}_g^1 = \{g(\tilde{L}) = \epsilon_1 I + \epsilon_2 \tilde{L} | \epsilon_2 \neq 0, g([0, 2]) \in [0, 1], \sum_i g(\lambda_i) > 1\}$ as a family of first-order graph filters and $\mathcal{S}_g^2 = \{g(\tilde{L}) = \epsilon'_1 I + \epsilon'_2 \tilde{L} + \epsilon'_3 \tilde{L}^2 | \epsilon'_3 < 0, g([0, 2]) \in [0, 1], \sum_i g(\lambda_i) > 1\}$ as the family of second-order graph filters. We say g_1 with $\epsilon_2 < 0$ is a low-pass filter and g_1 with $\epsilon_2 > 0$ is a high-pass filter. Similarly, since $g_2(\tilde{L}) = \epsilon'_3(\frac{\epsilon'_2}{2\epsilon'_3}I + \tilde{L})^2 + (\epsilon'_1 - \frac{\epsilon'^2_2}{4\epsilon'_3})I$, we say g_2 with $-\frac{\epsilon'_2}{2\epsilon'_3} < 1$, i.e., $\epsilon'_2 + 2\epsilon'_3 < 0$ is a low-pass filter and g_2 with $\epsilon'_2 + 2\epsilon'_3 > 0$ is a high-pass filter.

Theorem 5.5 (Low/high-pass). *Given a graph \mathcal{G}_n with interaction probability $\tilde{\Pi}$, let $g_1 = \arg \max_{g \in \mathcal{S}_g^1} \mathcal{H}_1(\tilde{g}(I - \tilde{\Pi})|\mathcal{G}_n)$ and $g_2 = \arg \max_{g \in \mathcal{S}_g^2} \mathcal{H}_1(\tilde{g}(I - \tilde{\Pi})|\mathcal{G}_n)$,*

- when $\mathcal{H}_1(\tilde{\Pi}|\mathcal{G}_n) > 0$, g_1, g_2 must be low-pass,
- when $\mathcal{H}_1(\tilde{\Pi}|\mathcal{G}_n) < 0$, g_1, g_2 must be high-pass.

Moreover, denote $A = \frac{(\sqrt{R_0} - \sqrt{R_1})^2}{n}$, we have

$$\begin{aligned}\mathcal{H}_1(\tilde{g}_1(I - \tilde{\Pi})|\mathcal{G}_n) &= \frac{A}{2} \int_0^2 g_1 d\lambda + |\epsilon_2 \mathcal{H}_1(\tilde{\Pi}|\mathcal{G}_n)|, \\ \mathcal{H}_1(\tilde{g}_2(I - \tilde{\Pi})|\mathcal{G}_n) &= \frac{A}{2} \int_0^2 g_2 d\lambda + \epsilon'_3 (\mathcal{H}_2(\tilde{\Pi}|\mathcal{G}_n) - \frac{A}{3}) + |(\epsilon'_2 + 2\epsilon'_3) \mathcal{H}_1(\tilde{\Pi}|\mathcal{G}_n)|.\end{aligned}$$

This theorem rigorously validates our inference of Proposition 4.9: **low-pass filters are superior to high-pass filters on homophilic graphs**. Compared with first-order filters, second-order filters involve 2-homophily degrees so that they can identify more different graphs. Actually, we show that second-order filters are easier to have better performance than first-order filters.

Theorem 5.6 (First/second-order). *Given a graph \mathcal{G}_n with interaction probability $\tilde{\Pi}$ and $a = \frac{2(\sqrt{R_0} - \sqrt{R_1})^2}{3n}$, for $g_1 \in \mathcal{S}_g^1$, there exists a $g_2 \in \mathcal{S}_g^2$ such that*

1. when $\mathcal{H}_2(\tilde{\Pi}|\mathcal{G}_n) \in [-1, a]$, $\mathcal{H}_1(\tilde{g}_2(I - \tilde{\Pi})|\mathcal{G}_n) > \mathcal{H}_1(\tilde{g}_1(I - \tilde{\Pi})|\mathcal{G}_n)$;
2. when $\mathcal{H}_2(\tilde{\Pi}|\mathcal{G}_n) \in [a, 1]$, $|\mathcal{H}_1(\tilde{g}_2(I - \tilde{\Pi})|\mathcal{G}_n) - \mathcal{H}_1(\tilde{g}_1(I - \tilde{\Pi})|\mathcal{G}_n)| \leq -\frac{\epsilon'_3}{3} \mathcal{H}_2(\tilde{\Pi}|\mathcal{G}_n)$.

It shows the superiority of second-order filters on most graphs apart from those with a high 2-homophily degree and gives a guarantee to narrow the disadvantage. There is an intuitive hyperthesis to be inferred from this theorem: **high-order filters have an advantage over low order filters in most cases**. However, high-order filters would bring high computation costs. In practice, to enhance the GNNs performance, filter banks are empirically used in previous works. Below, we provide a **rigorous demonstration of the advantage of filter banks**.

Theorem 5.7 (Filter bank). *Given a graph \mathcal{G}_n with normalized Laplacian matrix \tilde{L} with eigenvalues $\{\lambda_i\}$, $\forall g_1(\cdot)$ in \mathcal{S}_g^1 , there exists a single filter $g_2(\cdot) \in \mathcal{S}_g^1$ and positive l_1, l_2 s.t. for $g = l_1 g_1 + l_2 g_2$ we have*

$$\frac{m_{g_1}}{m_g} \log \frac{\mathcal{H}_1(\tilde{g}(I - \tilde{\Pi})|\mathcal{G}_n)}{\sum_i g(\lambda_i)} > \log \frac{\mathcal{H}_1(\tilde{g}_1(I - \tilde{\Pi})|\mathcal{G}_n)}{\sum_i g_1(\lambda_i)},$$

and $l_1 + l_2 = 1$, here $m_g = \min_{i \in \mathcal{I}_g} g(\lambda_i)$.

This theorem can be generalized to the family of second-order graph filters \mathcal{S}_g^2 .

5.3. A Strategy for Filter Design

According to our theoretical framework and conclusion on prediction error of a specific label, a graph filter that has a high response efficiency on this label difference or which can strengthen the internal connection of this class is the key to the success of GNNs. Considering a K -class classification problem, as we showed in Sect.3.1, we will obtain K related binary classification problems with K label differences. When these label differences have a high diversity of frequency distributions, a low order single filter is prone to fail since it can barely have high response efficiencies on all of them. In these cases, it is necessary to leverage a filter bank to handle different frequency distributions.

How to design a powerful filter bank efficiently? Theoretically, piling up sufficient numbers of graph filters to capture all the frequency components can improve prediction performance while it is very expensive. On the other hand, following our theoretical results, it is not difficult to design an ideal filter bank with the frequency distributions of label differences or graph interaction probability on hand. However, such graph indicators are usually unknown. Nevertheless, node features are accessible in attribute graphs and provide valid information for classification. As illustrated in Theorem 5.2, an ideal filter should have a high response frequency on both input difference and label difference. Here we assume that for each label there is some information provided by (partial) features useful for identification. Also, target frequency components and features may differ for different labels. When we classify labels with different target components having the same frequency, we need to separate objects with different target components before filtering. Otherwise, it is likely to bring noise and hurt the performance. Therefore, feature disentanglement is necessary. On the other hand, since a filter bank is applied to features to capture valid information, filter design should be targeted at specific graphs and features.

6. Model and Empirical Study

As already emphasized, one practical strategy for improving prediction performance is to learn a filter bank in a data-driven manner. In this section, to verify this theoretical strategy, we propose a simple framework - disentangled multi-filter framework (DEMUF)

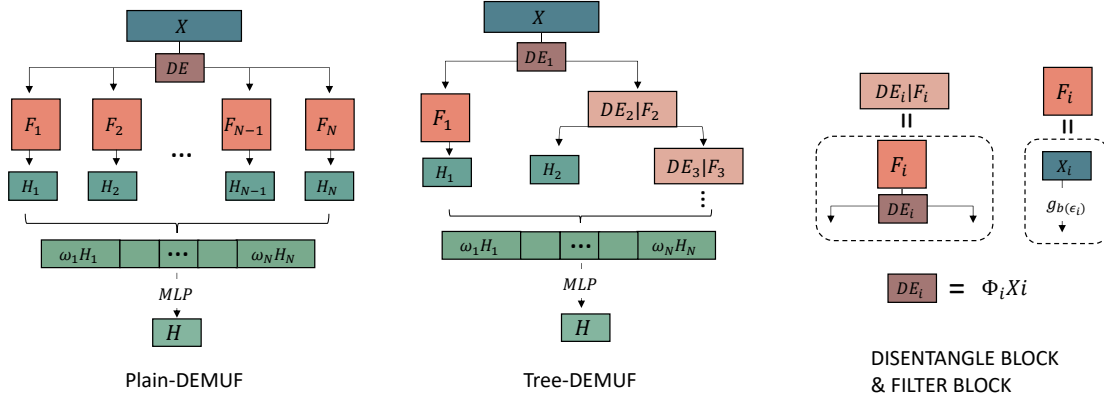


Figure 1. Illustration of Plain-DEMUF and Tree-DEMUF. There are two main model blocks of DEMUF frameworks: *disentangle block* and *filter block*. In Plain-DEMUF, all filter blocks run in parallel as their disentangled input are generated through a single disentangle block at the same time. Differently, each Tree-DEMUF layer contains two branches - one is early stopped while the other will be disentangled into two branches of the next layer after going through a filter.

6.1. Architecture of Two Frameworks of DEMUF

Following the conclusions in Sect.5.3, i.e., different features should be assigned to different filters, we assemble **feature disentanglement** and **frequency filtering** blocks to our framework. The block of feature disentanglement is to divide features into different families in a learnable way. Then in the frequency filtering block, learnable graph filters are applied to targeted families of features. We provide two frameworks with different structures: Plain-DEMUF and Tree-DEMUF (depicted in Fig. 1).

The DISENTANGLE block and FILTER block are formulated as follows:

$$X_k = \text{DISENTANGLE}(X, \Phi_k) = \Phi_k(X),$$

$$H_k = \text{FILTER}(X_k, \epsilon_k, h_k) = (g_{\epsilon_k}(\tilde{L}))^{h_k} X_k.$$

In our implementation, we provide two samples of DISENTANGLE functions Φ_k : one is linear transformations, the other is GUMBEL_SOFTMAX (Jang et al., 2017) used to generate learnable masks for feature selection. In terms of the FILTER block, we use the normalized second order filter $g_\epsilon(\tilde{L}) = I - \frac{((1-\epsilon)I - \tilde{L})^2}{(1+|\epsilon|)^2}$ with learnable parameter $\epsilon \in (-1, 1)$. In each FILTER block, h is the number of layers. The framework of Plain-DEMUF with N filters is:

$$H_k = \text{FILTER}\left(\text{DISENTANGLE}\left(X, \Phi_k\right), \epsilon_k, h_k\right),$$

$$H = \text{MLP}\left(\text{CONCAT}\left(\left\{H_k, \omega_k \mid k = 1, \dots, N\right\}\right)\right).$$

Based on this, we implement a simple model called P-DEMUF. Precisely, we leverage a GUMBEL_SOFTMAX to generate N learnable masks $\{M_1, \dots, M_N\}$ for feature sampling at once followed by different MLP. That is, $\Phi_k(X) = \text{MLP}_k(X \odot M_k)$.

Similarly, we develop a model, T-DEMUF, under the framework of Tree-DEMUF formulated by:

$$X_1 = \text{FILTER}\left(\text{DISENTANGLE}\left(X, \Psi_1\right), \epsilon_1, h_1\right),$$

$$H_1 = \text{FILTER}\left(\text{DISENTANGLE}\left(X, \Phi_1\right), \epsilon, h\right),$$

$$\begin{aligned}
 H_{k+1} &= \text{DISENTANGLE}(X_k, \Phi_k), \\
 X_{k+1} &= \text{FILTER}\left(\text{DISENTANGLE}(X_k, \Psi_k), \epsilon_k, h_k\right), \\
 H &= \text{MLP}\left(\text{CONCAT}\left(\left\{\omega_k H_k, k = 1, \dots, N\right\}\right)\right).
 \end{aligned}$$

In each T-DEMUF layer, we use GUMBEL_SOFTMAX with different parameters to generate two masks M_k and M'_k and $\Phi_k(X_k) = X_k \odot M_k$ and $\Psi_k(X_k) = X_k \odot M'_k$. In each layer, we stop further disentangling of the branch of H_k by utilizing an additional constraint

$$\mathcal{L}(X_{k-1}, H_k) = \|X_{k-1} \odot M'_k - H_k\|_2^2.$$

Noting that $H_k = (g_{\epsilon_k}(\tilde{L}))^{h_k} X_{k-1} \odot M'_k$, this constraint is to make $(g_{\epsilon_k}(\tilde{L}))^{h_k}$ has high response efficiency on H_k .

Model discussion. Compared with filter-bank learning methods which directly apply an array of filters to features, our models use subsets of features. It can greatly reduce the amount of computation and parameters and help learning filters more effectively. T-DEMUF uses an additional constraint to guide the filter learning process while filters in P-DEMUF do not interfere with each other. We provide further discussion and ablation study in Appendix A.

6.2. Experiments

To validate DEMUF, we compare the performances of P-DEMUF and T-DEMUF with that of spectral GNNs, spatial GNNs and MLP on extensive datasets.

6.2.1. EXPERIMENT SETTINGS

Datasets. We use various types of real datasets including two graphs of *Citation network* (Sen et al., 2008) - Cora and Citeseer; three subgraphs of *WebKB* (Pei et al., 2020) - Cornell, Texas, and Wisconsin; two *Wikipedia network* - Chameleon and Squirrel (Rozemberczki et al., 2021); two *relabelled Wikipedia network* proposed by Bo et al. (2021) - Chameleon2 and Squirrel2; and one graph of *Actor co-occurrence network* - Actor (Tang et al., 2009), to validate our proposed models. More statistics of datasets and the experimental setup can be found in Appendix A.

Baselines. We compare our models with four spectral GNNs: GCN (Kipf & Welling, 2017), ChebNet (Defferrard et al., 2016), GIN (Xu et al., 2019), ARMA (Bianchi et al., 2021). We list their spectral filter forms in Appendix A. In addition, we also add four spatial GNNs: GAT (Veličković et al., 2018), FAGCN (Bo et al., 2021), Geom_GCN (Pei et al., 2020) and GPRGNN (Chien et al., 2020). Both GAT and FAGCN utilize attention mechanism, Geom_GCN is a novel aggregation method based on the geometry of graph, GPRGNN can handle both homophilic and heterophilic graphs through learning GPR weights. Finally, we also compare with MLP which is an all-pass filter.

Table 1. Node classification accuracy. The first row is the homophily degree.

	Cora	Cite.	Cornell	Texas	Wisc.	Cham.	Squi.	Cham.2	Squi.2	Actor	
$\mathcal{H}_1(\tilde{\Pi} \mathcal{G}_n)$	0.637	0.586	0.103	0.072	0.018	-0.116	-0.279	0.127	0.044	-0.215	
Spectral	GCN	88.50	76.20	69.02	66.07	58.50	64.11	47.60	75.49	70.87	32.89
	Cheby	88.21	76.26	81.97	82.79	82.50	63.61	50.93	77.68	69.13	37.23
	GIN	87.06	74.10	56.89	69.84	51.25	37.42	23.73	58.10	49.24	29.64
	ARMA	87.56	74.86	85.25	85.25	92.63	69.34	51.60	78.93	73.95	35.49
Spatial	GAT	88.32	76.85	60.82	72.30	61.63	66.17	44.75	77.18	69.67	36.40
	FAGCN	89.19	77.15	73.51	65.41	76.86	61.70	39.70	76.10	66.70	34.61
	Gemo_GCN	85.27	77.90	60.81	67.57	64.12	60.90	38.14	73.20	63.30	31.63
	GPRGNN	/	/	91.36	92.92	/	67.48	49.93	/	/	39.30
Ours	MLP	75.33	71.40	92.46	92.46	95.00	49.56	34.89	77.28	63.19	37.38
	T-DEMUF	86.72	74.57	92.97	92.79	93.21	72.03	59.09	83.31	74.92	41.11
	P-DEMUF	87.85	75.69	91.60	92.04	94.38	71.47	57.58	82.40	74.54	39.18
	v.s. Spectral	↓0.65	↓0.57	↑7.72	↑7.54	↑1.75	↑2.69	↑7.49	↑4.38	↑0.97	↑3.88
v.s. all	↓1.34	↓2.21	↑0.51	↓0.13	↓0.625	↑2.69	↑7.49	↑4.38	↑0.97	↑1.81	

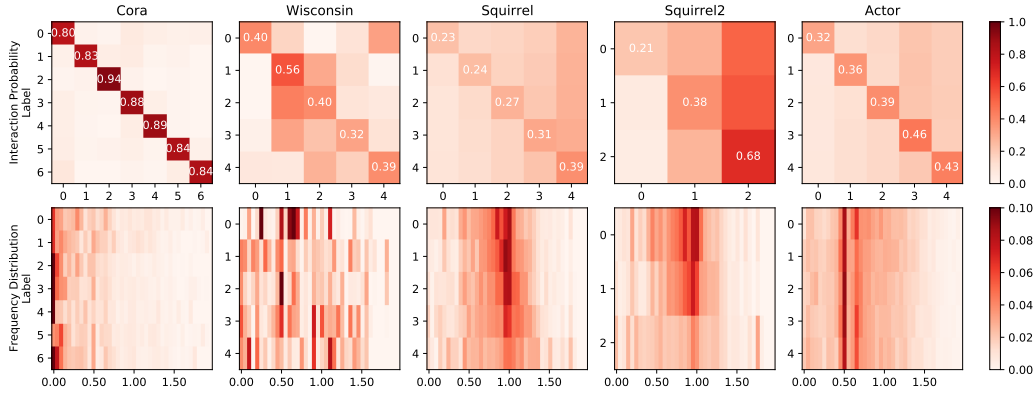


Figure 2. Visualizations of interaction probability matrix and label frequency distribution of five datasets.

6.3. Result and Analysis

We summarize the experimental results in Table 1 and visualize the interaction probability and label frequency distribution of some typical graphs in Fig. 2.

Our models show consistent superiority on most benchmarks and outperform all spectral GNN baselines. These promising results strongly suggest that our strategy of filter design proposed in Sect.5.3 is effective to improve spectral GNNs’ prediction performance. Precisely, T-DEMUF yields over 7.49% higher accuracy than the best baselines (ARMA) on Squirrel. Compared with baselines with first-order filters (GCN and GIN), our models and other baselines with high-order filters (Cheby and ARMA) have a huge lead on most of datasets apart from Cora and Citeseer. It empirically validates our argument about the superiority of high-order filters proposed in Theorem 5.6. On the other hand, the poor performance of GCN and GIN we implemented which are low-pass filters on graphs with low homophily degree verify our analysis on low-pass filters provided by Theorem 5.5. In addition, the visualization of Cora’s indicators confirms our deduction in Sect.4.2 - high interaction probability brings high homophily degree and high concentration of label frequency distribution on low-frequency.

Interestingly, all models have poor performance on Actor (less than 42%) while partial models including T-DEMUF, P-DEMUF obtain over 90% prediction accuracy on WebKB networks and all have good results on Cora. We indicate that these observations strongly support our theoretical analysis on prediction error in terms of graph indicators in Sect.5.1.1 and 5.1.2. For example: 1. high homophily degree makes Cora easy to be classified; 2. highly diverse label frequency distributions which imply high label difference information content give a guarantee of good performance of appropriate filters on Wisconsin; 3. low homophily degree and similar label frequency distributions of Actor make all models fail.

7. Conclusion

In this paper, we conduct a theoretical analysis on the prediction error of spectral GNNs and develop a deep analysis of graph filters’ performance based on the introduction of significant graph indicators. We also propose an effective and practical strategy for filter design which has been empirically validated by a simple framework we developed.

References

Balcilar, M., Renton, G., Héroux, P., Gaüzère, B., Adam, S., and Honeine, P. Analyzing the expressive power of graph neural networks in a spectral perspective. In *International Conference on Learning Representations*, 2020.

Bianchi, F. M., Grattarola, D., Livi, L., and Alippi, C. Graph neural networks with convolutional arma filters. *IEEE Transactions on Pattern Analysis and Machine Intelligence*, 2021.

Bo, D., Wang, X., Shi, C., and Shen, H. Beyond low-frequency information in graph convolutional networks. In *Thirty-Fifth AAAI Conference on Artificial Intelligence*, pp. 3950–3957, 2021.

- Bruna, J., Zaremba, W., Szlam, A., and LeCun, Y. Spectral networks and deep locally connected networks on graphs. In *International Conference on Learning Representations*, 2014.
- Chang, H., Rong, Y., Xu, T., Huang, W., Sojoudi, S., Huang, J., and Zhu, W. Spectral graph attention network. *arXiv preprint arXiv:2003.07450*, 2020.
- Chien, E., Peng, J., Li, P., and Milenkovic, O. Adaptive universal generalized pagerank graph neural network. *arXiv preprint arXiv:2006.07988*, 2020.
- Defferrard, M., Bresson, X., and Vandergheynst, P. Convolutional neural networks on graphs with fast localized spectral filtering. In *Advances in Neural Information Processing Systems*, pp. 3844–3852, 2016.
- Gao, X., Dai, W., Li, C., Zou, J., Xiong, H., and Frossard, P. Message passing in graph convolution networks via adaptive filter banks. *arXiv preprint arXiv:2106.09910*, 2021.
- Jang, E., Gu, S., and Poole, B. Categorical reparameterization with gumbel-softmax. In *International Conference on Learning Representations*, 2017.
- Jin, D., Yu, Z., Huo, C., Wang, R., Wang, X., He, D., and Han, J. Universal graph convolutional networks. *Advances in Neural Information Processing Systems*, 34, 2021.
- Kipf, T. N. and Welling, M. Semi-supervised classification with graph convolutional networks. In *International Conference on Learning Representations*, 2017.
- Ma, Y., Liu, X., Shah, N., and Tang, J. Is homophily a necessity for graph neural networks? *arXiv preprint arXiv:2106.06134*, 2021.
- Min, Y., Wenkel, F., and Wolf, G. Scattering gcn: Overcoming oversmoothness in graph convolutional networks. *Advances in Neural Information Processing Systems*, 33, 2020.
- Nt, H. and Maehara, T. Revisiting graph neural networks: All we have is low-pass filters. *arXiv preprint arXiv:1905.09550*, 2019.
- Oono, K. and Suzuki, T. Graph neural networks exponentially lose expressive power for node classification. In *International Conference on Learning Representations*, 2020.
- Ortega, A., Frossard, P., Kovacevic, J., Moura, J. M. F., and Vandergheynst, P. Graph signal processing: Overview, challenges, and applications. *Proc. IEEE*, 106(5):808–828, 2018. doi: 10.1109/JPROC.2018.2820126. URL <https://doi.org/10.1109/JPROC.2018.2820126>.
- Pei, H., Wei, B., Chang, K. C.-C., Lei, Y., and Yang, B. Geom-gcn: Geometric graph convolutional networks. In *International Conference on Learning Representations*, 2020.
- Rozemberczki, B., Allen, C., and Sarkar, R. Multi-scale attributed node embedding. *Journal of Complex Networks*, 9(2), 2021.
- Sen, P., Namata, G., Bilgic, M., Getoor, L., Galligher, B., and Eliassi-Rad, T. Collective classification in network data. *AI Magazine*, 29(3):93–93, 2008.
- Tang, J., Sun, J., Wang, C., and Yang, Z. Social influence analysis in large-scale networks. In *Proceedings of the 15th ACM SIGKDD International Conference on Knowledge Discovery and Data Mining*, pp. 807–816, 2009.
- Veličković, P., Cucurull, G., Casanova, A., Romero, A., Lio, P., and Bengio, Y. Graph attention networks. In *International Conference on Learning Representations*, 2018.
- Xu, K., Hu, W., Leskovec, J., and Jegelka, S. How powerful are graph neural networks? In *International Conference on Learning Representations*, 2019.
- Zhu, J., Yan, Y., Zhao, L., Heimann, M., Akoglu, L., and Koutra, D. Beyond homophily in graph neural networks: Current limitations and effective designs. In *Advances in Neural Information Processing Systems*, 2020.

A. Benchmarks and Model Discussion

A.1. Statistics information of benchmarks.

We use four types of real datasets - *Citation network*, *WebKB*, *Actor co-occurrence network* and *Wikipedia network*, to validate our proposed models. Cora and Citeseer (Sen et al., 2008) are widely used citation benchmarks which represent paper as nodes and citation between two papers as edges. Cornell, Texas, and Wisconsin (Pei et al., 2020) are three subgraphs of WebKB which is a webpage network with web pages as nodes and hyperlinks between them as edges. Chameleon and Squirrel (Rozenberczki et al., 2021) are two Wikipedia networks with web pages as nodes and links between pages as edges. The nodes originally have five classes while Bo et al. (2021) proposed a new classification criteria which divides nodes into three main categories. In this paper, the relabeled networks are called Chameleon2 and Squirrel2. Actor (Tang et al., 2009) is a subgraph of the film-director-actor-writer network whose nodes only represent actors and edges represent their collaborations.

We provide statistics information of our benchmarks in Table. A.1.

Table 2. Datasets statistics.

Dataset	Cora	Cite.	Cornell	Texas	Wisc.	Cham.	Squi.	Cham.2	Squi.2	Actor
# Nodes	2708	3327	183	183	251	2277	5201	2277	5201	7600
# Edges	5429	4732	295	309	499	36101	217073	36101	217073	33544
# Features	1433	3703	1703	1703	1703	2325	2089	2325	2089	931
# Classes	7	6	5	5	5	5	5	3	3	5

A.2. Spectral filters.

In our paper, we use four spectral GNNs as baselines whose spectral filters are listed as Table.A.2 and define a normalized second order filter $g_\epsilon(\tilde{L})$ with $\epsilon \in [-1, 1]$.

Table 3. Spectral filters.

Model	Filter
GCN	$I - \tilde{L}$
GIN	$(2 + \epsilon)I - \tilde{L}$
ChebNet	$C^{(s)} = 2C^{(2)}C^{(s-1)} - C^{(s-2)}$; $C^{(2)} = 2L/\lambda_{max} - I$; $C_1 = I$
ARMA	$(I + \sum_{k=1}^K q^k L^k)^{-1} (\sum_{k=0}^{K-1} p_k L^k)$
Ours	$I - \frac{((1-\epsilon)I - \tilde{L})^2}{(1+ \epsilon)^2}$

Noting that $g_\epsilon(\tilde{L}) = I - \frac{((1-\epsilon)I - \tilde{L})^2}{(1+|\epsilon|)^2} = \frac{((2+|\epsilon|-\epsilon)I - \tilde{L})((|\epsilon|+\epsilon)I + \tilde{L})}{(1+|\epsilon|)^2}$, it is exactly an overlap between a low-pass filter $(2 + |\epsilon| - \epsilon)I - \tilde{L}$ and a high-pass filter $(|\epsilon| + \epsilon)I + \tilde{L}$.

For a given graph \mathcal{G}_n with interaction probability $\tilde{\Pi}$, we investigate $\mathcal{H}_1(\tilde{g}(I - \tilde{\Pi})|\mathcal{G}_n)$ for our second-order filter and the filter of GCN. We first normalize GCN’s filter as $g_{gcn}(\tilde{L}) = I - \frac{\tilde{L}}{2}$, then we have

$$\begin{aligned} \mathcal{H}_1(\tilde{g}_{gcn}(I - \tilde{\Pi})|\mathcal{G}_n) &= \frac{(R_0 - R_1)^2}{2n} + \frac{1}{2}\mathcal{H}_1(\tilde{\Pi}|\mathcal{G}_n) \\ \mathcal{H}_1(\tilde{g}_\epsilon(I - \tilde{\Pi})|\mathcal{G}_n) &= \frac{1 + 2|\epsilon|}{(1 + |\epsilon|)^2} \frac{(R_0 - R_1)^2}{n} + \frac{2\epsilon\mathcal{H}_1(\tilde{\Pi}|\mathcal{G}_n) - \mathcal{H}_2(\tilde{\Pi}|\mathcal{G}_n)}{(1 + |\epsilon|)^2} \end{aligned}$$

A.3. Model Discussion.

How can our filter bank selection be data-driven.

As we clarified in Sect.6, our implementation of disentanglement is not random masking but learnable masking leveraging GUMBEL-SOFTMAX. These learnable maskings disentangle node features into several subsets of features. In our algorithm,

although the form of our second order filter $g_\epsilon(\tilde{L})$ is predefined, its parameters including ϵ and weight ω are learned from specified graphs. Moreover, the parameters of our feature disentanglement blocks (the linear transformations and learnable masking) are also learned from data which will affect the learning of the filter bank. Therefore, our filter bank selection is data-driven.

A.4. Experimental Setup and Additional Results

Experimental Setup.

For all data, we use 60% nodes for training, 20% for validation and 20% for testing. For all experiments, we report the mean prediction accuracy on the testing data for 10 runs. We search learning rate, hidden unit, weight decay and dropout for all models in the same search space. Finally, we choose learning rate of 0.01, dropout rate of 0.5, and hidden unit of 64 over all datasets. The number of filters are searched between 2 to 10, and the final setting is: both T-DEMUF and P-DEMUF use 2 filters with 1 layer and 3-layer MLP on WebKB; 2 filters with 18 layers and 3-layer MLP on Wikipedia and 5 filters with 1 layer and 4-layer MLP on Actor. For Citation networks, T-DEMUF uses 4 filters with 7 layers while P-DEMUF uses 3 filters with 8 layers. In addition, as the setting of benchmarks are the same as that in Geom_GCN, we refer to the results reported in (Pei et al., 2020).

Ablation Study.

To show the advantage of using disentanglement, we provide an ablation study on five benchmarks. Here, we propose two ablation models based on P-DEMUF. Recall that the disentanglement block of P-DEMUF consists of learnable masking and linear transformations, we design our ablation models by taking off the component of masking and linear transformation. Also, for fair and intuitive comparison, we simply fix the number of filters as 2. The results shown as Table.A.4 validate that if we take off the disentanglement blocks of P-DEMUF, the results become worse in most of benchmarks.

Table 4. Node classification accuracy of P-DEMUF and its ablation models. We fix the number of second order filters as 2.

Dataset	Cornell	Texas	Cham.	Squi.	Actor
P-DEMUF	81.08	85.14	68.46	55.45	36.95
P-DEMUF (w/o masking)	80.00	84.86	67.20	53.54	37.20
P-DEMUF (w/o masking & linear)	77.30	86.49	62.5	44.19	36.71

B. Proof of Theorem

B.1. Proof of Theorem 3.2

Before presenting the proof of Theorem 3.2, we start with a useful lemma.

Lemma B.1. Denote $x \in \mathbb{R}$, $y \in \{0, 1\}$, $\mathcal{S}(x, y) = \{x < -1, y = 1 \text{ or } x > 1, y = 0\}$ and ψ is the clamp function defined as

$$\psi(x) = \min\{\max\{x, -1\}, 1\} = \begin{cases} 1 & x > 1 \\ x & -1 < x < 1 \\ -1 & x < -1 \end{cases},$$

then we have

$$\left(\frac{1}{1+e^x} - y\right)^2 \geq \frac{1}{4} - \frac{(1-2y)\psi(x)}{4} + \frac{\psi(x)^2}{16} - \frac{|\psi(x)|^3}{48} - \frac{|\psi(x)|^4}{96} - \frac{1}{(1+e)^2} \mathbf{1}_{\mathcal{S}(x, y)},$$

where, $\mathbf{1}_{\mathcal{S}(x, y)}$ is the indication function of $\mathcal{S}(x, y)$.

Proof. Noting that

$$\text{error}(x, \psi(x)) = \left(\frac{1}{1+e^x} - y\right)^2 - \left(\frac{1}{1+e^{\psi(x)}} - y\right)^2 \in \begin{cases} [-(\frac{1}{1+e})^2, 0] & x > 1, y = 0 \\ [0, (\frac{1}{1+e})^2] & x > 1, y = 1 \\ [0, (\frac{1}{1+e})^2] & x < -1, y = 0 \\ [-(\frac{1}{1+e})^2, 0] & x < -1, y = 1 \end{cases}$$

then we have

$$error(x, \psi(x)) \geq -\frac{1}{(1+e)^2} \mathbf{1}_S(x, y).$$

For $x \in [-1, 1]$, the first-order (also the second order) Taylor expansion of $\frac{1}{1+e^x}$ is $\frac{1}{2} - \frac{1}{4}x$.

Denote $R(x)$ as the remainder term, i.e. $R(x) = \frac{1}{1+e^x} - \frac{1}{2} + \frac{1}{4}x$, since

$$\left(\frac{1}{(1+e^x)^2}\right)''' = -\frac{e^x(-4e^x + e^{2x} + 1)}{(1+e^x)^4} \leq \left(\frac{1}{(1+e^x)^2}\right)''' \Big|_{x=0} = \frac{1}{8},$$

we have

$$|R(x)| \leq \max \left| \left(\frac{1}{(1+e^x)^2}\right)''' \right| \frac{|x|^3}{3!} = \frac{|x|^3}{48}.$$

Therefore,

$$\begin{aligned} \left(\frac{1}{1+e^x} - y\right)^2 &= \left(\frac{1}{1+e^{\psi(x)}} - y\right)^2 + error(x, \psi(x)) \\ &\geq \left(\frac{1}{1+e^{\psi(x)}} - y\right)^2 - \frac{1}{(1+e)^2} \mathbf{1}_S(x, y) \\ &= \left(\frac{1}{2} - \frac{1}{4}\psi(x) - y + R(\psi(x))\right)^2 - \frac{1}{(1+e)^2} \mathbf{1}_S(x, y) \\ &\geq \left(\frac{1}{2} - \frac{1}{4}\psi(x) - y\right)^2 - 2|R(\psi(x))| \left|\frac{1}{2} - \frac{1}{4}\psi(x) - y\right| - \frac{1}{(1+e)^2} \mathbf{1}_S(x, y) \\ &\geq \left(\frac{1}{2} - \frac{1}{4}\psi(x) - y\right)^2 - \frac{|\psi(x)|^3}{24} \left|\frac{1}{2} - \frac{1}{4}\psi(x) - y\right| - \frac{1}{(1+e)^2} \mathbf{1}_S(x, y) \\ &\geq \left(\frac{1}{2} - \frac{1}{4}\psi(x) - y\right)^2 - \frac{|\psi(x)|^3}{48} - \frac{|\psi(x)|^4}{96} - \frac{1}{(1+e)^2} \mathbf{1}_S(x, y) \\ &= \frac{1}{4} - \frac{(1-2y)\psi(x)}{4} + \frac{\psi(x)^2}{16} - \frac{|\psi(x)|^3}{48} - \frac{|\psi(x)|^4}{96} - \frac{1}{(1+e)^2} \mathbf{1}_S(x, y) \end{aligned}$$

□

Below, we provide the proof of Theorem 3.2.

Proof of Theorem 3.2

Proof. According to Lemma B.1,

$$\begin{aligned} Er(\mathbf{x}_0, \mathbf{y}_0) &= \left\| \frac{e^{g(\tilde{L})\mathbf{x}_0}}{e^{g(\tilde{L})\mathbf{x}_0} + e^{g(\tilde{L})\mathbf{x}_1}} - \mathbf{y}_0 \right\|_2^2 = \sum_l \left(\frac{1}{1 + e^{g(\tilde{L})(\mathbf{x}_{1l} - \mathbf{x}_{0l})}} - \mathbf{y}_{0l} \right)^2 \\ &\geq \sum_l \frac{1}{4} - \frac{(1-2\mathbf{y}_{0l})\psi(\mathbf{z}_l)}{4} + \frac{\psi(\mathbf{z}_l)^2}{16} - \frac{|\psi(\mathbf{z}_l)|^3}{48} - \frac{|\psi(\mathbf{z}_l)|^4}{96} - \frac{I_S(\mathbf{z}_l, y)}{(1+e)^2} \\ &= \frac{n}{4} + \frac{\|\psi(\mathbf{z})\|_2^2}{16} - \frac{1}{2} \left(\frac{1}{2} - \mathbf{y}_0\right)^\top \psi(\mathbf{z}) - \frac{C}{(1+e)^2} - \sum_l \frac{|\psi(\mathbf{z}_l)|^3}{24} \left|\frac{1}{2} - \frac{1}{4}\psi(\mathbf{z}_l) - \mathbf{y}_{0l}\right| \\ &\geq \frac{n}{4} - \frac{1}{4}(\mathbf{y}_1 - \mathbf{y}_0)^\top \psi(\mathbf{z}) + \frac{\|\psi(\mathbf{z})\|_2^2}{16} - \frac{\|\psi(\mathbf{z})\|_3^3}{48} - \frac{\|\psi(\mathbf{z})\|_4^4}{96} - \frac{C}{(1+e)^2} \\ &= \tilde{Er}(\mathbf{x}_0, \mathbf{y}_0). \end{aligned}$$

Noting that $C \leq \|\psi(\mathbf{z})\|_4 \leq \|\psi(\mathbf{z})\|_3 \leq \|\psi(\mathbf{z})\|_2 \leq n$, then we have

$$\begin{aligned}
 \tilde{E}r(\mathbf{x}_0, \mathbf{y}_0) &\geq \left(\frac{n}{4} - \frac{\|\psi(\mathbf{z})\|_3^3}{32}\right) + \left(\frac{1}{16} - \frac{1}{(1+e)^2}\right)C - \frac{1}{4}(\mathbf{y}_1 - \mathbf{y}_0)^\top \psi(\mathbf{z}) \\
 &> \frac{n}{4} - \frac{\|\psi(\mathbf{z})\|_3^3}{32} - \frac{C}{100} - \frac{1}{4}(\mathbf{y}_1 - \mathbf{y}_0)^\top \psi(\mathbf{z}) \\
 &> \frac{n}{4} - \frac{33}{800} \|\psi(\mathbf{z})\|_3^3 - \frac{1}{4}(\mathbf{y}_1 - \mathbf{y}_0)^\top \psi(\mathbf{z}) \\
 &> \frac{167}{800}n - \frac{1}{4}(\mathbf{y}_1 - \mathbf{y}_0)^\top \psi(\mathbf{z}) \\
 &= \frac{167}{800}n - \frac{1}{4}(\mathbf{y}_1 - \mathbf{y}_0)^\top \psi(g(\tilde{L})(\mathbf{x}_1 - \mathbf{x}_0)) \\
 &= \frac{167}{800}n - \frac{1}{4} \sum_l \psi((\mathbf{y}_{1l} - \mathbf{y}_{0l})(g(\tilde{L})(\mathbf{x}_1 - \mathbf{x}_0)_l)).
 \end{aligned}$$

□

B.2. Proof of Proposition 4.4 and 4.9

We first introduce two useful lemma.

Lemma B.2. For $\mathcal{G} = \{\mathcal{V}, \mathcal{E}\}$, let \mathbf{f} be the frequency of signal \mathbf{x} , then $\mathbb{E}[\mathbf{f}^n] = \frac{\mathbf{x}^\top (I - \tilde{A})^n \mathbf{x}}{\mathbf{x}^\top \mathbf{x}}$.

Proof. Since $\mathbf{x} = \sum_{i=0}^{n-1} \alpha_i \mathbf{u}_i$, \mathbf{u}_i is the i -th unit eigenvector of \tilde{L} and $\lambda^n = \mathbf{u}_i^\top \tilde{L}^n \mathbf{u}_i$ then we have

$$\mathbb{E}[\mathbf{f}^n] = \sum_{i=0}^{n-1} P(\mathbf{f} = \lambda_i) \lambda_i^n = \frac{\sum (\alpha_i \mathbf{u}_i)^\top \tilde{L}^n (\alpha_i \mathbf{u}_i)}{\sum \alpha_i^2} = \frac{\mathbf{x}^\top \tilde{L}^n \mathbf{x}}{\mathbf{x}^\top \mathbf{x}} = \frac{\mathbf{x}^\top (I - \tilde{A})^n \mathbf{x}}{\mathbf{x}^\top \mathbf{x}}.$$

□

Lemma B.3. Let $B \in \mathbb{R}^{n \times n}$ is a symmetric matrix, $\forall i, j, \mathbf{y} \in \mathbb{R}^n$, we have

$$\frac{\mathbf{y}^\top B^2 \mathbf{y}}{\mathbf{y}^\top \mathbf{y}} \geq \left(\frac{\mathbf{y}^\top B \mathbf{y}}{\mathbf{y}^\top \mathbf{y}}\right)^2.$$

Proof. Since B is symmetric, then we have $B = U \Lambda U^\top$, here U is matrix of unit eigenvectors of B . From the proof of Lemma B.2, we obtain that $\frac{\mathbf{y}^\top B^2 \mathbf{y}}{\mathbf{y}^\top \mathbf{y}} = \frac{\sum (\alpha_i \lambda_i)^2}{\sum \alpha_i^2}$ and $\left(\frac{\mathbf{y}^\top B \mathbf{y}}{\mathbf{y}^\top \mathbf{y}}\right)^2 = \left(\frac{\sum \alpha_i^2 \lambda_i}{\sum \alpha_i^2}\right)^2$.

From Hölder's inequality, we have $(\sum (\alpha_i \lambda_i)^2)(\sum \alpha_i^2) \geq (\sum \alpha_i^2 \lambda_i)^2$.

Therefore, we have $\frac{\sum (\alpha_i \lambda_i)^2}{\sum \alpha_i^2} \geq \frac{(\sum \alpha_i^2 \lambda_i)^2}{(\sum \alpha_i^2)^2}$. □

Below is the proof of Proposition 4.4.

Proof of proposition 4.4.

Proof. For $P = D^{-1}A$ and $\tilde{A} = D^{-\frac{1}{2}}AD^{-\frac{1}{2}}$, and $\Pi, \tilde{\Pi}$ defined by Definition 4.1,

$$\begin{aligned}
 R_l \Pi_{lm}^k + R_m \Pi_{ml}^k &\geq \sqrt{R_l R_m} \tilde{\Pi}_{lm}^k \\
 \iff (R \Pi^k + (\Pi^k)^\top R)_{lm} &\geq 2(R^{\frac{1}{2}} \tilde{\Pi}^k R^{\frac{1}{2}})_{lm} \\
 \iff \mathbf{y}_m^\top (P^k + (P^k)^\top) \mathbf{y}_l &\geq 2 \mathbf{y}_m^\top \tilde{A}^k \mathbf{y}_l \\
 \iff \mathbf{y}_m^\top (P^k + D P^k D^{-1}) \mathbf{y}_l &\geq 2 \mathbf{y}_m^\top D^{\frac{1}{2}} P^k D^{-\frac{1}{2}} \mathbf{y}_l \\
 \iff \mathbf{y}_m^\top (P^k + D P^k D^{-1} - 2 D^{\frac{1}{2}} P^k D^{-\frac{1}{2}}) \mathbf{y}_l &\geq 0
 \end{aligned}$$

Since $(P^k + (P^k)^\top)_{ij} = P_{ij}^k + \frac{d_i}{d_j} P_{ij}^k \geq 2\sqrt{\frac{d_i}{d_j}} P_{ij}^k = 2\tilde{A}_{ij}^k$, we have $\mathbf{y}_m^\top (P^k + (P^k)^\top - 2\tilde{A}^k) \mathbf{y}_l \geq 0$.

Let $m = l$, then we get $\pi_l^k \geq \tilde{\pi}_l^k$.

According to Lemma B.3, let $g(\cdot) = (\cdot)^n$, since $g(\tilde{A})$ is symmetric, then we have

$$(g^2[\tilde{\Pi}])_{ll} = \frac{\mathbf{y}^\top (g(\tilde{A}))^2 \mathbf{y}}{\mathbf{y}^\top \mathbf{y}} \geq \left(\frac{\mathbf{y}^\top g(\tilde{A}) \mathbf{y}}{\mathbf{y}^\top \mathbf{y}} \right)^2 = (g[\tilde{\Pi}]_{ll})^2 \Rightarrow \tilde{\pi}_l^{2k} \geq (\tilde{\pi}_l^k)^2.$$

□

Proof of Proposition 4.9.

Proposition 4.9 can be directly derived from Lemma B.2.

B.3. Proof of Theorem 5.2 and 5.4

Denote indicator set $\mathcal{I}_g = \{i | g(\lambda_i) \neq 0, i = 0, \dots, n-1\}$, $\mathcal{I}_\delta = \{i | \delta_i \neq 0, i = 0, \dots, n-1\}$ and $\mathcal{I}_{g,\delta} = \mathcal{I}_g \cap \mathcal{I}_\delta$, it is obvious that $\sum_{i=0}^{n-1} \psi(\eta_i g(\lambda_i) \delta_i) = \sum_{i \in \mathcal{I}_{g,\delta,\eta}} \psi(\eta_i g(\lambda_i) \delta_i)$. For any η , we construct $\tilde{\eta}_i = \psi_{\frac{1}{g(\lambda_i) \delta_i}}(\eta_i)$ such that $|\tilde{\eta}_i g(\lambda_i) \delta_i| \leq 1$ and $\sum_{i \in \mathcal{I}_{g,\delta,\eta}} \psi(\eta_i g(\lambda_i) \delta_i) = \sum_{i \in \mathcal{I}_{g,\delta,\tilde{\eta}}} \tilde{\eta}_i g(\lambda_i) \delta_i$.

Lemma B.4. For any $g(\cdot)$ and δ ,

$$\sum_{i \in \mathcal{I}_{g,\delta}} g(\lambda_i) \leq \frac{\sum_{i \in \mathcal{I}_{g,\delta}} \log p_i}{\log(1 + c(g, \delta)) \mu_g(\delta)} \leq \frac{\sum_{i \in \mathcal{I}_\delta} \log p_i}{\log(1 + c(g, \delta)) \mu_g(\delta)}, \quad (11)$$

here $c(g, \delta) = \frac{\sum_{i \in \mathcal{I}_g - \mathcal{I}_{g,\delta}} g(\lambda_i)}{\sum_{i \in \mathcal{I}_{g,\delta}} g(\lambda_i)}$ and $p_i = \frac{\delta_i^2}{\sum_{k=0}^{n-1} \delta_k^2}$.

Proof. According to the weighted AM-GM inequality, we have

$$\begin{aligned} \frac{\sum_{i \in \mathcal{I}_{g,\delta}} g(\lambda_i) p_i}{\sum_{i \in \mathcal{I}_{g,\delta}} g(\lambda_i)} &\geq \prod_{i \in \mathcal{I}_{g,\delta}} p_i^{\frac{g(\lambda_i)}{\sum_{k \in \mathcal{I}_{g,\delta}} g(\lambda_k)}} \geq \left(\prod_{i \in \mathcal{I}_{g,\delta}} p_i \right)^{\frac{1}{\sum_{k \in \mathcal{I}_{g,\delta}} g(\lambda_k)}} \\ \Rightarrow \sum_{i \in \mathcal{I}_{g,\delta}} g(\lambda_i) &\leq \frac{\sum_{i \in \mathcal{I}_{g,\delta}} \log p_i}{\log \sum_{i \in \mathcal{I}_{g,\delta}} g(\lambda_i) p_i - \log \sum_{i \in \mathcal{I}_{g,\delta}} g(\lambda_i)} \end{aligned}$$

Noting that $\mu_g(\delta) = \frac{\sum_{i=0}^{n-1} g(\lambda_i) p_i}{\sum_{i=0}^{n-1} g(\lambda_i)} = \frac{\sum_{i \in \mathcal{I}_{g,\delta}} g(\lambda_i) p_i}{\sum_{i \in \mathcal{I}_g} g(\lambda_i)}$, we have

$$\frac{\sum_{i \in \mathcal{I}_{g,\delta}} g(\lambda_i) p_i}{\sum_{i \in \mathcal{I}_{g,\delta}} g(\lambda_i)} = \frac{\sum_{i \in \mathcal{I}_g} g(\lambda_i)}{\sum_{i \in \mathcal{I}_{g,\delta}} g(\lambda_i)} \mu_g(\delta) = \left(1 + \frac{\sum_{i \in \mathcal{I}_g - \mathcal{I}_{g,\delta}} g(\lambda_i)}{\sum_{i \in \mathcal{I}_{g,\delta}} g(\lambda_i)} \right) \mu_g(\delta) = (1 + c(g, \delta)) \mu_g(\delta) < 1,$$

here $c(g, \delta) = \frac{\sum_{i \in \mathcal{I}_g - \mathcal{I}_{g,\delta}} g(\lambda_i)}{\sum_{i \in \mathcal{I}_{g,\delta}} g(\lambda_i)}$.

Then we obtain that

$$\sum_{i \in \mathcal{I}_{g,\delta}} g(\lambda_i) \leq \frac{\sum_{i \in \mathcal{I}_{g,\delta}} \log p_i}{\log(1 + c(g, \delta)) \mu_g(\delta)} \leq \frac{\sum_{i \in \mathcal{I}_\delta} \log p_i}{\log(1 + c(g, \delta)) \mu_g(\delta)}.$$

□

Corollary B.5. For any $g(\cdot)$, δ and $\tilde{\eta}$ with $p_i = \frac{\delta_i^2}{\sum_{k=0}^{n-1} \delta_k^2}$ and $q_i = \frac{\tilde{\eta}_i^2}{\sum_{k=0}^{n-1} \tilde{\eta}_k^2}$, we have

$$\sum_{i \in \mathcal{I}_{g,\delta,\tilde{\eta}}} g(\lambda_i) \leq \min \left\{ \frac{\sum_{i \in \mathcal{I}_{g,\delta}} \log p_i}{\log(1 + c(g, \delta)) \mu_g(\delta)}, \frac{\sum_{i \in \mathcal{I}_{g,\tilde{\eta}}} \log q_i}{\log(1 + c(g, \tilde{\eta})) \mu_g(\tilde{\eta})} \right\}. \quad (12)$$

Proof. Since $g(\lambda_i) \in [0, 1]$, $\mathcal{I}_{g,\delta,\tilde{\eta}} \subseteq \mathcal{I}_{g,\delta}$ and $\mathcal{I}_{g,\delta,\tilde{\eta}} \subseteq \mathcal{I}_{g,\tilde{\eta}}$, then

$$\sum_{i \in \mathcal{I}_{g,\delta,\tilde{\eta}}} g(\lambda_i) \leq \min\left\{ \sum_{i \in \mathcal{I}_{g,\delta}} g(\lambda_i), \sum_{i \in \mathcal{I}_{g,\tilde{\eta}}} g(\lambda_i) \right\}.$$

With this observation and Lemma B.4, we can obtain the corollary. \square

Below is the proof of Theorem 5.2 and 5.4.

Proof of Theorem 5.2.

Proof. Since $m_g = \min_{i \in \mathcal{I}_{g,\delta,\tilde{\eta}}} g(\lambda_i) > 0$, $\max_{i \in \mathcal{I}_{g,\delta,\tilde{\eta}}} |\tilde{\eta}_i \delta_i| \leq \frac{1}{m_g}$. With Lemma B.1 and its corollary B.5, we obtain the upper bound of $\sum_{i=0}^{n-1} \psi(\eta_i g(\lambda_i) \delta_i)$:

$$\begin{aligned} \sum_{i=0}^{n-1} \psi(\eta_i g(\lambda_i) \delta_i) &= \sum_{i \in \mathcal{I}_{g,\delta,\tilde{\eta}}} \psi(\eta_i g(\lambda_i) \delta_i) = \sum_{i \in \mathcal{I}_{g,\delta,\tilde{\eta}}} \tilde{\eta}_i g(\lambda_i) \delta_i \\ &\leq \sum_{i \in \mathcal{I}_{g,\delta,\tilde{\eta}}} g(\lambda_i) |\tilde{\eta}_i \delta_i| \leq \frac{\sum_{i \in \mathcal{I}_{g,\delta,\tilde{\eta}}} g(\lambda_i)}{m_g} \\ &\leq \frac{1}{m_g} \min\left\{ \frac{\sum_{i \in \mathcal{I}_{g,\delta}} \log p_i}{\log(1 + c(g, \delta)) \mu_g(\delta)}, \frac{\sum_{i \in \mathcal{I}_{g,\tilde{\eta}}} \log q_i}{\log(1 + c(g, \tilde{\eta})) \mu_g(\tilde{\eta})} \right\} \\ &\leq \frac{1}{m_g} \min\left\{ \frac{\sum_{i \in \mathcal{I}_\delta} \log p_i}{\log(1 + c(g, \delta)) \mu_g(\delta)}, \frac{\sum_{i \in \mathcal{I}_{\tilde{\eta}}} \log q_i}{\log(1 + c(g, \tilde{\eta})) \mu_g(\tilde{\eta})} \right\} \\ &= \frac{1}{m_g} \min\left\{ \frac{-\mathbf{I}(\delta)}{\log(1 + c(g, \delta)) \mu_g(\delta)}, \frac{-\mathbf{I}(\tilde{\eta})}{\log(1 + c(g, \tilde{\eta})) \mu_g(\tilde{\eta})} \right\} \end{aligned}$$

\square

Proof of Theorem 5.4.

Proof. Let $\Delta y = \mathbf{y}_0 - \mathbf{y}_1$ and γ, ω be the spectra of \mathbf{y}_0 and \mathbf{y}_1 , respectively. Then $\delta = \gamma - \omega$.

Since $\|\gamma - \omega\|_2^2 = \|\mathbf{y}_0 - \mathbf{y}_1\|_2^2 = n$, $\mathbf{I}(\gamma - \omega) = \sum_i \log \frac{(\gamma_i - \omega_i)^2}{\|\gamma - \omega\|_2^2} = 2 \sum_i \log |\gamma_i - \omega_i| - n \log n$.

Denote p_i as the frequency probability of Δy , according to the definition, we have $p_i = \frac{(\gamma_i - \omega_i)^2}{\|\gamma - \omega\|_2^2} = \frac{\gamma_i^2 + \omega_i^2 - 2\gamma_i \omega_i}{n}$. Recall the definition of the measure $\mu_g(\cdot)$ and symmetric interaction probability, we represent $\mu_g(\delta)$ as:

$$\begin{aligned} \mu_g(\delta) &= \frac{\sum_i g(\lambda_i) p_i}{\sum_i g(\lambda_i)} \\ &= \frac{\sum_i g(\lambda_i) (\gamma_i^2 + \omega_i^2 - 2\gamma_i \omega_i)}{n \sum_i g(\lambda_i)} \\ &= \frac{\gamma^\top g(\Lambda) \gamma + \omega^\top g(\Lambda) \omega - 2\gamma^\top g(\Lambda) \omega}{n \sum_i g(\lambda_i)} \\ &= \frac{\mathbf{y}_0^\top g(\tilde{L}) \mathbf{y}_0 + \mathbf{y}_1^\top g(\tilde{L}) \mathbf{y}_1 - 2\mathbf{y}_0^\top g(\tilde{L}) \mathbf{y}_1}{n \sum_i g(\lambda_i)} \\ &= \frac{R_0(\tilde{g}(I - \tilde{\Pi}))_{00} + R_1 \tilde{g}(I - \tilde{\Pi})_{11} - 2\sqrt{R_0 R_1} \tilde{g}(I - \tilde{\Pi})_{01}}{n \sum_i g(\lambda_i)} \end{aligned}$$

As we show in the proof of Lemma B.4,

$$(1 + c(g, \delta)) \mu_g(\delta) = \frac{\sum_{i \in \mathcal{I}_g} g(\lambda_i)}{\sum_{i \in \mathcal{I}_{g,\delta}} g(\lambda_i)} \mu_g(\delta).$$

Since $\sum_{i \in \mathcal{I}_g} g(\lambda_i) = \sum_i g(\lambda_i)$, we have

$$\begin{aligned} & (1 + c(g, \delta))\mu_g(\delta) \\ &= \frac{R_0(\tilde{g}(I - \tilde{\Pi}))_{00} + R_1\tilde{g}(I - \tilde{\Pi})_{11} - 2\sqrt{R_0R_1}\tilde{g}(I - \tilde{\Pi})_{01}}{n \sum_{i \in \mathcal{I}_{g,\delta}} g(\lambda_i)} \\ &= \frac{\mathcal{H}_1(\tilde{g}(I - \tilde{\Pi})|\mathcal{G}_n)}{\sum_{i \in \mathcal{I}_{g,\delta}} g(\lambda_i)}. \end{aligned}$$

Based on the Corollary 5.3, we have

$$Er(X, Y) = 2Er(\mathbf{x}_0, \mathbf{y}_0) > \frac{167}{400}n + \frac{\mathbf{I}(\delta)}{2m_g \log \frac{\mathcal{H}_1(\tilde{g}(I - \tilde{\Pi})|\mathcal{G}_n)}{\sum_i g(\lambda_i)}}.$$

□

B.4. Proof of Theorem 5.5 and 5.6

Proof of Theorem 5.5.

Proof. To prove this theorem is equivalent to prove that for $g_1(\tilde{L}) = \epsilon_1 I + \epsilon_2 \tilde{L} \in \mathcal{S}_g^1$ and $g_2(\tilde{L}) = \epsilon'_1 I + \epsilon'_2 \tilde{L} + \epsilon'_3 \tilde{L}^2 \in \mathcal{S}_g^2$, then for homophilic graphs with $\mathcal{H}_1(\tilde{\Pi}|\mathcal{G}_n) > 0$, we can always find a low-pass filter work better than a high-pass filter; otherwise, we can always find a high-pass filter work better than a low-pass filter.

Denote $\int_0^2 g_1(\lambda)d\lambda = 2(\epsilon_1 + \epsilon_2) = a$ and $\int_0^2 g_2(\lambda)d\lambda = \epsilon'_1 + \epsilon'_2 + \frac{4}{3}\epsilon'_3 = b$, then we have

$$\begin{aligned} \mathcal{H}_1(\tilde{g}_1(I - \tilde{\Pi})|\mathcal{G}_n) &= \frac{R_0}{n}(\tilde{g}_1(I - \tilde{\Pi}))_{00} + \frac{R_1}{n}(\tilde{g}_1(I - \tilde{\Pi}))_{11} - 2\frac{\sqrt{R_0R_1}}{n}(\tilde{g}_1(I - \tilde{\Pi}))_{01} \\ &= (\epsilon_1 + \epsilon_2)\frac{(\sqrt{R_0} - \sqrt{R_1})^2}{n} - \epsilon_2\frac{(R_0\tilde{\pi}_0 + R_1\tilde{\pi}_1 - 2\sqrt{R_0R_1}\tilde{\Pi}_{01})}{n} \\ &= (\epsilon_1 + \epsilon_2)\left(1 - \frac{2\sqrt{R_0R_1}}{n}\right) - \epsilon_2\mathcal{H}_1(\tilde{\Pi}|\mathcal{G}_n) \\ &= \frac{a}{2}\left(1 - \frac{2\sqrt{R_0R_1}}{n}\right) - \epsilon_2\mathcal{H}_1(\tilde{\Pi}|\mathcal{G}_n) \\ \mathcal{H}_1(\tilde{g}_2(I - \tilde{\Pi})|\mathcal{G}_n) &= \frac{R_0}{n}(\tilde{g}_2(I - \tilde{\Pi}))_{00} + \frac{R_1}{n}(\tilde{g}_2(I - \tilde{\Pi}))_{11} - 2\frac{\sqrt{R_0R_1}}{n}(\tilde{g}_2(I - \tilde{\Pi}))_{01} \\ &= (\epsilon'_1 + \epsilon'_2 + \epsilon'_3)\frac{(\sqrt{R_0} - \sqrt{R_1})^2}{n} - (\epsilon'_2 + 2\epsilon'_3)\frac{(R_0\tilde{\pi}_0 + R_1\tilde{\pi}_1 - 2\sqrt{R_0R_1}\tilde{\Pi}_{01})}{n} \\ &\quad + \epsilon'_3\frac{(R_0\tilde{\pi}_0^2 + R_1\tilde{\pi}_1^2 - 2\sqrt{R_0R_1}\tilde{\Pi}_{01}^2)}{n} \\ &= (\epsilon'_1 + \epsilon'_2 + \epsilon'_3)\left(1 - \frac{2\sqrt{R_0R_1}}{n}\right) - (\epsilon'_2 + 2\epsilon'_3)\mathcal{H}_1(\tilde{\Pi}|\mathcal{G}_n) + \epsilon'_3\mathcal{H}_2(\tilde{\Pi}|\mathcal{G}_n) \\ &= \left(\frac{b}{2} - \frac{1}{3}\epsilon'_3\right)\left(1 - \frac{2\sqrt{R_0R_1}}{n}\right) - (\epsilon'_2 + 2\epsilon'_3)\mathcal{H}_1(\tilde{\Pi}|\mathcal{G}_n) + \epsilon'_3\mathcal{H}_2(\tilde{\Pi}|\mathcal{G}_n) \end{aligned}$$

Given a graph with $\mathcal{H}_1(\tilde{\Pi}|\mathcal{G}_n) > 0$, for a given first-order high-pass filter $g(\tilde{L}) = \epsilon_1 I + |\epsilon_2|\tilde{L}$, we can always find a low-pass filter such as $g'(\tilde{L}) = (\epsilon_1 + 2|\epsilon_2|)I - |\epsilon_2|\tilde{L}$ such that

$$\mathcal{H}_1(\tilde{g}(I - \tilde{\Pi})|\mathcal{G}_n) < \mathcal{H}_1(g'(I - \tilde{\Pi})|\mathcal{G}_n) = \frac{a}{2}\left(1 - \frac{2\sqrt{R_0R_1}}{n}\right) + |\epsilon_2|\mathcal{H}_1(\tilde{\Pi}|\mathcal{G}_n).$$

For a given second order high-pass filter $g(\tilde{L}) = \epsilon'_1 I + \epsilon'_2 \tilde{L} + \epsilon'_3 \tilde{L}^2$ with $\epsilon'_2 + 2\epsilon'_3 > 0$, we can always find a low-pass filter such as $g'(\tilde{L}) = (\epsilon'_1 + 2\epsilon'_2 + 4\epsilon'_3)I - (\epsilon'_2 + 4\epsilon'_3)\tilde{L} + \epsilon'_3 \tilde{L}^2$ such that

$$\mathcal{H}_1(\tilde{g}(I - \tilde{\Pi})|\mathcal{G}_n) < \mathcal{H}_1(g'(I - \tilde{\Pi})|\mathcal{G}_n) = \left(\frac{b}{2} - \frac{1}{3}\epsilon'_3\right)\left(1 - \frac{2\sqrt{R_0 R_1}}{n}\right) + (\epsilon'_2 + 2\epsilon'_3)\mathcal{H}_1(\tilde{\Pi}|\mathcal{G}_n) + \epsilon'_3 \mathcal{H}_2(\tilde{\Pi}|\mathcal{G}_n).$$

Similarly, Given a graph with $\mathcal{H}_1(\tilde{\Pi}|\mathcal{G}_n) < 0$, for a given first-order low-pass filter $g(\tilde{L}) = \epsilon_1 I - |\epsilon_2|\tilde{L}$, we can always find a high-pass filter such as $g'(\tilde{L}) = (\epsilon_1 - 2|\epsilon_2|)I + |\epsilon_2|\tilde{L}$ such that

$$\mathcal{H}_1(\tilde{g}(I - \tilde{\Pi})|\mathcal{G}_n) < \mathcal{H}_1(g'(I - \tilde{\Pi})|\mathcal{G}_n) = \frac{a}{2}\left(1 - \frac{2\sqrt{R_0 R_1}}{n}\right) + |\epsilon_2 \mathcal{H}_1(\tilde{\Pi}|\mathcal{G}_n)|.$$

For a given second order low-pass filter $g(\tilde{L}) = \epsilon'_1 I + \epsilon'_2 \tilde{L} + \epsilon'_3 \tilde{L}^2$ with $\epsilon'_2 + 2\epsilon'_3 < 0$, we can always find a high-pass filter such as $g'(\tilde{L}) = (\epsilon'_1 + 2\epsilon'_2 + 4\epsilon'_3)I - (\epsilon'_2 + 4\epsilon'_3)\tilde{L} + \epsilon'_3 \tilde{L}^2$ such that

$$\mathcal{H}_1(\tilde{g}(I - \tilde{\Pi})|\mathcal{G}_n) < \mathcal{H}_1(g'(I - \tilde{\Pi})|\mathcal{G}_n) = \left(\frac{b}{2} - \frac{1}{3}\epsilon'_3\right)\left(1 - \frac{2\sqrt{R_0 R_1}}{n}\right) + |(\epsilon'_2 + 2\epsilon'_3)\mathcal{H}_1(\tilde{\Pi}|\mathcal{G}_n)| + \epsilon'_3 \mathcal{H}_2(\tilde{\Pi}|\mathcal{G}_n).$$

Based on the above conclusions, for a given graph \mathcal{G}_n , for given filter g_1, g_2 there exists g'_1 and g'_2 such that

$$\begin{aligned} \mathcal{H}_1(\tilde{g}'_1(I - \tilde{\Pi})|\mathcal{G}_n) &= \frac{a}{2}\left(1 - \frac{2\sqrt{R_0 R_1}}{n}\right) + |\epsilon_2 \mathcal{H}_1(\tilde{\Pi}|\mathcal{G}_n)| \\ \mathcal{H}_1(\tilde{g}'_2(I - \tilde{\Pi})|\mathcal{G}_n) &= \left(\frac{b}{2} - \frac{1}{3}\epsilon'_3\right)\left(1 - \frac{2\sqrt{R_0 R_1}}{n}\right) + |(\epsilon'_2 + 2\epsilon'_3)\mathcal{H}_1(\tilde{\Pi}|\mathcal{G}_n)| + \epsilon'_3 \mathcal{H}_2(\tilde{\Pi}|\mathcal{G}_n). \end{aligned}$$

□

Proof of Theorem 5.6.

Proof. According to Theorem 5.5, for a given graph \mathcal{G}_n , for given filter g_1, g_2 there exists g'_1 and g'_2 such that

$$\begin{aligned} \mathcal{H}_1(\tilde{g}'_1(I - \tilde{\Pi})|\mathcal{G}_n) &= \frac{a}{2}\left(1 - \frac{2\sqrt{R_0 R_1}}{n}\right) + |\epsilon_2 \mathcal{H}_1(\tilde{\Pi}|\mathcal{G}_n)| \\ \mathcal{H}_1(\tilde{g}'_2(I - \tilde{\Pi})|\mathcal{G}_n) &= \left(\frac{b}{2} - \frac{1}{3}\epsilon'_3\right)\left(1 - \frac{2\sqrt{R_0 R_1}}{n}\right) + |(\epsilon'_2 + 2\epsilon'_3)\mathcal{H}_1(\tilde{\Pi}|\mathcal{G}_n)| + \epsilon'_3 \mathcal{H}_2(\tilde{\Pi}|\mathcal{G}_n). \end{aligned}$$

Since $\forall g_1 \in \mathcal{S}_g^1, g_2 \in \mathcal{S}_g^2, g_1([0, 2]) \in [0, 1]$ and $g_2([0, 2]) \in [0, 1]$, then we have $|\epsilon_2| \leq \frac{1}{2}$ and $|\epsilon_2 + 2\epsilon_3| \leq \frac{1}{2}$.

$$\begin{aligned} \mathcal{H}_1(\tilde{g}'_1(I - \tilde{\Pi})|\mathcal{G}_n) &\leq \frac{1}{2}\left(1 - \frac{2\sqrt{R_0 R_1}}{n}\right) + \frac{1}{2}|\mathcal{H}_1(\tilde{\Pi}|\mathcal{G}_n)| \\ \mathcal{H}_1(\tilde{g}'_2(I - \tilde{\Pi})|\mathcal{G}_n) &\leq \left(\frac{1}{2} - \frac{2}{3}\epsilon'_3\right)\left(1 - \frac{2\sqrt{R_0 R_1}}{n}\right) + \frac{1}{2}|\mathcal{H}_1(\tilde{\Pi}|\mathcal{G}_n)| + \epsilon'_3 \mathcal{H}_2(\tilde{\Pi}|\mathcal{G}_n). \end{aligned}$$

These inequalities hold when $\epsilon_1 = 1, |\epsilon_2| = \frac{1}{2}$ and $|\epsilon_2 + 2\epsilon_3| = \frac{1}{2}$. Let g_1 with $|\epsilon_2| = \frac{1}{2}$ and g_2 with $|\epsilon_2 + 2\epsilon_3| = \frac{1}{2}$, then we have

$$\begin{aligned} &\mathcal{H}_1(\tilde{g}'_2(I - \tilde{\Pi})|\mathcal{G}_n) - \mathcal{H}_1(\tilde{g}'_1(I - \tilde{\Pi})|\mathcal{G}_n) \\ &= \left(-\frac{2}{3}\epsilon'_3\right)\left(1 - \frac{2\sqrt{R_0 R_1}}{n}\right) + \epsilon'_3 \mathcal{H}_2(\tilde{\Pi}|\mathcal{G}_n) \\ &= -\frac{\epsilon'_3}{n}\left(R_0\left(\frac{2}{3} - \tilde{\pi}_0^2\right) + R_1\left(\frac{2}{3} - \tilde{\pi}_1^2\right) + 2\sqrt{R_0 R_1}\left(\frac{2}{3} - \tilde{\pi}_{01}^2\right)\right) \\ &\geq \frac{\epsilon'_3}{3}\mathcal{H}_2(\tilde{\Pi}|\mathcal{G}_n) \end{aligned}$$

Therefore, $\mathcal{H}_1(\tilde{g}'_2(I - \tilde{\Pi})|\mathcal{G}_n) > \mathcal{H}_1(\tilde{g}'_1(I - \tilde{\Pi})|\mathcal{G}_n)$ when $\mathcal{H}_2(\tilde{\Pi}|\mathcal{G}_n) < \frac{2}{3}\left(1 - \frac{2\sqrt{R_0 R_1}}{n}\right)$, otherwise then we have $|\mathcal{H}_1(\tilde{g}'_2(I - \tilde{\Pi})|\mathcal{G}_n) - \mathcal{H}_1(\tilde{g}'_1(I - \tilde{\Pi})|\mathcal{G}_n)| \leq -\frac{\epsilon'_3}{3}\mathcal{H}_2(\tilde{\Pi}|\mathcal{G}_n)$. □

B.5. Proof of Theorem 5.7

Lemma B.6. For any function $g(\cdot)$ which is nonnegative on the closed interval $[0, 2]$,

$$G(g, \tilde{\Pi}) = R_0(\tilde{g}(I - \tilde{\Pi}))_{00} + R_1\tilde{g}(I - \tilde{\Pi})_{11} - 2\sqrt{R_0R_1}\tilde{g}(I - \tilde{\Pi})_{01} > 0.$$

Proof.

$$\begin{aligned} & R_0(\tilde{g}(I - \tilde{\Pi}))_{00} + R_1\tilde{g}(I - \tilde{\Pi})_{11} - 2\sqrt{R_0R_1}\tilde{g}(I - \tilde{\Pi})_{01} \\ &= \mathbf{y}_0^\top g(\tilde{L})\mathbf{y}_0 + \mathbf{y}_1^\top g(\tilde{L})\mathbf{y}_1 - 2\mathbf{y}_0^\top g(\tilde{L})\mathbf{y}_1 \\ &= (\mathbf{y}_0 - \mathbf{y}_1)^\top g(\tilde{L})(\mathbf{y}_0 - \mathbf{y}_1) \end{aligned}$$

Since \tilde{L} is symmetric positive definite with eigenvalues falling in $[0, 2]$, for any nonnegative g , $g(\tilde{L})$ is also symmetric positive definite. Thus, $(\mathbf{y}_0 - \mathbf{y}_1)^\top g(\tilde{L})(\mathbf{y}_0 - \mathbf{y}_1) > 0$. \square

Proof of Theorem 5.7

Proof. Here we assume that $\mathcal{I}_{\gamma-\omega} = \emptyset$, that is for any g , $\mathcal{I}_{g,\gamma-\omega} = \mathcal{I}_g$. Below, we assume that $R_0 \neq R_1$.

It is easy to check that for any $g_1(\cdot), g_2(\cdot) \in \mathcal{S}_g$ and nonnegative constant l_1, l_2 with $l_1 + l_2 = 1$, $(l_1g_1 + l_2g_2)(\cdot) \in \mathcal{S}_g$.

For any $g \in \mathcal{S}_g$, $\tilde{g}(I - \tilde{\Pi}) = (\epsilon_1 + \epsilon_2)I - \epsilon_2\tilde{\Pi}$, thus

$$\begin{aligned} \frac{G(g, \tilde{\Pi})}{\sum_i g(\lambda_i)} &= \frac{R_0(\tilde{g}(I - \tilde{\Pi}))_{00} + R_1\tilde{g}(I - \tilde{\Pi})_{11} - 2\sqrt{R_0R_1}\tilde{g}(I - \tilde{\Pi})_{01}}{\sum_i (\epsilon_1 + \epsilon_2\lambda_i)} \\ &= \frac{(\epsilon_1 + \epsilon_2)(\sqrt{R_0} - \sqrt{R_1})^2 - \epsilon_2(R_0\tilde{\pi}_0 + R_1\tilde{\pi}_1 - 2\sqrt{R_0R_1}\tilde{\Pi}_{01})}{\epsilon_1n + \epsilon_2\sum_i \lambda_i} \end{aligned}$$

Denote $A(\tilde{\Pi}) = (\sqrt{R_0} - \sqrt{R_1})^2 \geq 0$, $B(\tilde{\Pi}) = R_0\tilde{\pi}_0 + R_1\tilde{\pi}_1 - 2\sqrt{R_0R_1}\tilde{\Pi}_{01}$, $C(\tilde{\Pi}) = \frac{A(\tilde{\Pi}) - B(\tilde{\Pi})}{A(\tilde{\Pi})}$ and $\bar{\lambda} = \frac{\sum_i \lambda_i}{n}$, then

$$\frac{G(g, \tilde{\Pi})}{n \sum_i g(\lambda_i)} = \frac{(\epsilon_1 + \epsilon_2)A(\tilde{\Pi}) - \epsilon_2B(\tilde{\Pi})}{(\epsilon_1 + \epsilon_2\bar{\lambda})n^2} = \frac{(\epsilon_1 + \epsilon_2C(\tilde{\Pi}))A}{(\epsilon_1 + \epsilon_2\bar{\lambda})n^2}.$$

If $\epsilon_2 > 0$, g is a high-pass filter and $m_g = \epsilon_1$; if $\epsilon_2 < 0$, g is a low-pass filter and $m_g = \epsilon_1 + \epsilon_2\lambda_{n-1}$ where λ_{n-1} is the maximal eigenvalue.

$$H(\epsilon_1, \epsilon_2) = m_g \log \frac{G(g, \tilde{\Pi})}{n \sum_i g(\lambda_i)} = \begin{cases} \epsilon_1 \log \frac{(\epsilon_1 + \epsilon_2C(\tilde{\Pi}))A}{(\epsilon_1 + \epsilon_2\bar{\lambda})n^2} & \epsilon_1 \in (0, 1), \epsilon_2 \in (0, \frac{1 - \epsilon_1}{2}) \\ (\epsilon_1 + \epsilon_2\lambda_{n-1}) \log \frac{(\epsilon_1 + \epsilon_2C(\tilde{\Pi}))A}{(\epsilon_1 + \epsilon_2\bar{\lambda})n^2} & \epsilon_1 \in (0, 1), \epsilon_2 \in (\frac{-\epsilon_1}{2}, 0) \end{cases}$$

Let $f(\epsilon_1, \epsilon_2) = \epsilon_1 \log \frac{(\epsilon_1 + \epsilon_2C(\tilde{\Pi}))A}{(\epsilon_1 + \epsilon_2\bar{\lambda})n^2}$ and $h(\epsilon_1, \epsilon_2) = \epsilon_2 \log \frac{(\epsilon_1 + \epsilon_2C(\tilde{\Pi}))A}{(\epsilon_1 + \epsilon_2\bar{\lambda})n^2}$, then we have:

$$\begin{aligned}
 \frac{\partial f}{\partial \epsilon_1} &= \frac{1}{\epsilon_1 + C(\tilde{\Pi})\epsilon_2} - \frac{1}{\epsilon_1 + \bar{\lambda}\epsilon_2}, & \frac{\partial f}{\partial \epsilon_2} &= \frac{C(\tilde{\Pi})}{\epsilon_1 + C(\tilde{\Pi})\epsilon_2} - \frac{\bar{\lambda}}{\epsilon_1 + \bar{\lambda}\epsilon_2}, \\
 \frac{\partial^2 f}{\partial \epsilon_1^2} &= \frac{\epsilon_1 + 2C(\tilde{\Pi})\epsilon_2}{(\epsilon_1 + C(\tilde{\Pi})\epsilon_2)^2} - \frac{\epsilon_1 + 2\bar{\lambda}\epsilon_2}{(\epsilon_1 + \bar{\lambda}\epsilon_2)^2}, & \frac{\partial^2 f}{\partial \epsilon_2^2} &= \frac{\bar{\lambda}^2\epsilon_1}{(\epsilon_1 + \bar{\lambda}\epsilon_2)^2} - \frac{(C(\tilde{\Pi}))^2\epsilon_1}{(\epsilon_1 + C(\tilde{\Pi})\epsilon_2)^2}, \\
 \frac{\partial^2 f}{\partial \epsilon_1 \epsilon_2} &= \frac{(C(\tilde{\Pi}))^2\epsilon_2}{(\epsilon_1 + C(\tilde{\Pi})\epsilon_2)^2} - \frac{\bar{\lambda}^2\epsilon_2}{(\epsilon_1 + \bar{\lambda}\epsilon_2)^2}, & \frac{\partial^2 h}{\partial \epsilon_1^2} &= \frac{\epsilon_2}{(\epsilon_1 + \bar{\lambda}\epsilon_2)^2} - \frac{\epsilon_2}{(\epsilon_1 + C(\tilde{\Pi})\epsilon_2)^2}, \\
 \frac{\partial^2 h}{\partial \epsilon_2^2} &= C(\tilde{\Pi}) \frac{2\epsilon_1 + C(\tilde{\Pi})\epsilon_2}{(\epsilon_1 + C(\tilde{\Pi})\epsilon_2)^2} - \bar{\lambda} \frac{2\epsilon_1 + \bar{\lambda}\epsilon_2}{(\epsilon_1 + \bar{\lambda}\epsilon_2)^2}, & \frac{\partial^2 h}{\partial \epsilon_1 \epsilon_2} &= \frac{\epsilon_1}{(\epsilon_1 + C(\tilde{\Pi})\epsilon_2)^2} - \frac{\epsilon_1}{(\epsilon_1 + \bar{\lambda}\epsilon_2)^2}
 \end{aligned}$$

According to Lemma B.6,

$$\begin{aligned}
 \frac{A(\tilde{\Pi}) - B(\tilde{\Pi})}{A(\tilde{\Pi})} &= \frac{(\sqrt{R_0} - \sqrt{R_1})^2 - R_0\tilde{\pi}_0 - R_1\tilde{\pi}_1 + 2\sqrt{R_0R_1}\tilde{\Pi}_{01}}{(\sqrt{R_0} - \sqrt{R_1})^2} \\
 &= \frac{R_0(1 - \tilde{\pi}_0) + R_1(1 - \tilde{\pi}_1) - 2\sqrt{R_0R_1}(1 - \tilde{\Pi}_{01})}{(\sqrt{R_0} - \sqrt{R_1})^2} > 0
 \end{aligned}$$

When $C(\tilde{\Pi}) \leq \bar{\lambda}$, $\epsilon_2 < 0$ is better.

I. $A(\tilde{\Pi}) \neq 0$ and $\epsilon_2 > 0$

The Hessian determinant of $H(\epsilon_1, \epsilon_2)$ is :

$$Hess(H) = \frac{\bar{\lambda}^2\epsilon_1^2(1 - \bar{\lambda})}{(\epsilon_1 + \bar{\lambda}\epsilon_2)^4} + \frac{(C(\tilde{\Pi}))^2\epsilon_1^2(1 - C(\tilde{\Pi}))}{(\epsilon_1 + C(\tilde{\Pi})\epsilon_2)^4}.$$

When $B(\tilde{\Pi}) < 0$, $C(\tilde{\Pi}) < 1$, then $Hess(H) > 0$, $H(\epsilon_1, \epsilon_2)$ is a convex function;

when $B(\tilde{\Pi}) > 0$, $C(\tilde{\Pi}) > 1 > \bar{\lambda}$, then $Hess(H)$ can be positive or negative.

$$\begin{cases}
 \frac{\partial H}{\partial \epsilon_1} = \log \frac{(\epsilon_1 + \epsilon_2 C(\tilde{\Pi}))A}{(\epsilon_1 + \epsilon_2 \bar{\lambda})n^2} + \frac{\epsilon_1}{\epsilon_1 + C(\tilde{\Pi})\epsilon_2} - \frac{\epsilon_1}{\epsilon_1 + \bar{\lambda}\epsilon_2}, \\
 \frac{\partial H}{\partial \epsilon_2} = \frac{C(\tilde{\Pi})\epsilon_1}{\epsilon_1 + C(\tilde{\Pi})\epsilon_2} - \frac{\bar{\lambda}\epsilon_1}{\epsilon_1 + \bar{\lambda}\epsilon_2},
 \end{cases}$$

Since $A(\tilde{\Pi}) = R_0 + R_1 - 2\sqrt{R_0R_1} \leq n$, therefore $H(\epsilon_1, \epsilon_2)$ has no stationary point.

- a. When $C(\tilde{\Pi}) > 1 > \bar{\lambda}$, $\frac{\partial H}{\partial \epsilon_2} > 0$, then fix ϵ_1 , H is monotonic increasing function w.r.t $\epsilon_2 \in (0, \frac{1-\epsilon_1}{2})$.

In this case, for any $g_1(\tilde{L}) = \epsilon_1 + \epsilon_2$, there exist $\epsilon'_2 \in (\epsilon_2, \frac{1-\epsilon_1}{2})$ such that for any positive constant l ,

$$H(\epsilon_1, l\epsilon_2 + (1-l)\epsilon'_2) > H(\epsilon_1\epsilon_2).$$

- b. When $C(\tilde{\Pi}) < \bar{\lambda}$, $\frac{\partial H}{\partial \epsilon_2} < 0$, then fix ϵ_1 , H is monotonic decreasing function w.r.t $\epsilon_2 \in (0, \frac{1-\epsilon_1}{2})$.

In this case, for any $g_1(\tilde{L}) = \epsilon_1 + \epsilon_2$, there exist $\epsilon'_2 \in (0, \epsilon_2)$ such that for any positive constant l ,

$$H(\epsilon_1, l\epsilon_2 + (1-l)\epsilon'_2) > H(\epsilon_1\epsilon_2).$$

- c. When $C(\tilde{\Pi}) = \bar{\lambda}$, $\frac{\partial H}{\partial \epsilon_1} = \log \frac{A}{n^2} < 0$, then fix ϵ_2 , H is monotonic decreasing function w.r.t $\epsilon_1 \in (0, 1]$.

In this case, for any $g_1(\tilde{L}) = \epsilon_1 + \epsilon_2$, there exist $\epsilon'_1 \in (0, \epsilon_1)$ such that for any positive constant l ,

$$H(l\epsilon_1 + (1-l)\epsilon'_1, \epsilon_2) > H(\epsilon_1\epsilon_2).$$

II. $A(\tilde{\Pi}) \neq 0$ and $\epsilon_2 < 0$

Since,

$$\begin{cases} \frac{\partial H}{\partial \epsilon_1} = \log \frac{(\epsilon_1 + \epsilon_2 C(\tilde{\Pi}))A}{(\epsilon_1 + \epsilon_2 \bar{\lambda})n^2} + \frac{\epsilon_1 + \epsilon_2 \lambda_{n-1}}{\epsilon_1 + C(\tilde{\Pi})\epsilon_2} - \frac{\epsilon_1 + \epsilon_2 \lambda_{n-1}}{\epsilon_1 + \bar{\lambda}\epsilon_2}, \\ \frac{\partial H}{\partial \epsilon_2} = \lambda_{n-1} \log \frac{(\epsilon_1 + \epsilon_2 C(\tilde{\Pi}))A}{(\epsilon_1 + \epsilon_2 \bar{\lambda})n^2} + \frac{C(\tilde{\Pi})(\epsilon_1 + \epsilon_2 \lambda_{n-1})}{\epsilon_1 + C(\tilde{\Pi})\epsilon_2} - \frac{\bar{\lambda}(\epsilon_1 + \epsilon_2 \lambda_{n-1})}{\epsilon_1 + \bar{\lambda}\epsilon_2}, \end{cases}$$

Similarly, $H(\epsilon_1, \epsilon_2)$ has no stationary point.

- a. When $C(\tilde{\Pi}) > 1 > \bar{\lambda}$, $\frac{\partial H}{\partial \epsilon_1} < 0$, then fix ϵ_2 , H is monotonic decreasing function w.r.t $\epsilon_1 \in (0, 1]$.

In this case, for any $g_1(\tilde{L}) = \epsilon_1 + \epsilon_2$, there exist $\epsilon'_1 \in (0, \epsilon_1)$ such that for any positive constant l ,

$$H(l\epsilon_1 + (1-l)\epsilon'_1, \epsilon_2) > H(\epsilon_1, \epsilon_2).$$

- b. When $C(\tilde{\Pi}) \leq \bar{\lambda}$, $\frac{\partial H}{\partial \epsilon_2} < 0$, then fix ϵ_1 , H is monotonic decreasing function w.r.t $\epsilon_2 \in (0, \frac{1-\epsilon_1}{2})$.

In this case, for any $g_1(\tilde{L}) = \epsilon_1 + \epsilon_2$, there exist $\epsilon'_2 \in (0, \epsilon_2)$ such that for any positive constant l ,

$$H(\epsilon_1, l\epsilon_2 + (1-l)\epsilon'_2) > H(\epsilon_1, \epsilon_2).$$

III. $A(\tilde{\Pi}) \neq 0$

When $A(\tilde{\Pi}) = 0$, since $A(\tilde{\Pi}) - B(\tilde{\Pi}) > 0$, then $B(\tilde{\Pi}) < 0$,

$$H(\epsilon_1, \epsilon_2) = m_g \log \frac{G(g, \tilde{\Pi})}{n \sum_i g(\lambda_i)} = \begin{cases} \epsilon_1 \log \frac{-\epsilon_2 B(\tilde{\Pi})}{(\epsilon_1 + \epsilon_2 \bar{\lambda})n^2} & \epsilon_1 \in (0, 1], \epsilon_2 \in (0, \frac{1-\epsilon_1}{2}] \\ (\epsilon_1 + \epsilon_2 \lambda_{n-1}) \log \frac{-\epsilon_2 B(\tilde{\Pi})}{(\epsilon_1 + \epsilon_2 \bar{\lambda})n^2} & \epsilon_1 \in (0, 1], \epsilon_2 \in (\frac{-\epsilon_1}{2}, 0) \end{cases}$$

- a. $\epsilon_2 > 0$

$$\begin{cases} \frac{\partial H}{\partial \epsilon_1} = \log \frac{-\epsilon_2 B(\tilde{\Pi})}{(\epsilon_1 + \epsilon_2 \bar{\lambda})n^2} - \frac{\epsilon_1}{\epsilon_1 + \bar{\lambda}\epsilon_2} < 0, \\ \frac{\partial H}{\partial \epsilon_2} = \frac{\epsilon_1}{\epsilon_2} - \frac{\bar{\lambda}\epsilon_1}{\epsilon_1 + \bar{\lambda}\epsilon_2} > 0, \end{cases}$$

Fix ϵ_1 , H is monotonic increasing function w.r.t $\epsilon_2 \in (0, \frac{1-\epsilon_1}{2})$. In this case, for any $g_1(\tilde{L}) = \epsilon_1 + \epsilon_2$, there exist $\epsilon'_2 \in (\epsilon_2, \frac{1-\epsilon_1}{2})$ such that for any positive constant l , $H(\epsilon_1, l\epsilon_2 + (1-l)\epsilon'_2) > H(\epsilon_1, \epsilon_2)$.

- b. $\epsilon_2 < 0$

$$\begin{cases} \frac{\partial H}{\partial \epsilon_1} = \log \frac{-\epsilon_2 B(\tilde{\Pi})}{(\epsilon_1 + \epsilon_2 \bar{\lambda})n^2} - \frac{\epsilon_1 + \epsilon_2 \lambda_{n-1}}{\epsilon_1 + \bar{\lambda}\epsilon_2} < 0, \\ \frac{\partial H}{\partial \epsilon_2} = \lambda_{n-1} \log \frac{-\epsilon_2 B(\tilde{\Pi})}{(\epsilon_1 + \epsilon_2 \bar{\lambda})n^2} + \frac{\epsilon_1 + \lambda_{n-1}}{\epsilon_2} - \frac{\bar{\lambda}(\epsilon_1 + \epsilon_2 \lambda_{n-1})}{\epsilon_1 + \bar{\lambda}\epsilon_2}, \end{cases}$$

Fix ϵ_2 , H is monotonic decreasing function w.r.t $\epsilon_1 \in (0, 1]$. In this case, for any $g_1(\tilde{L}) = \epsilon_1 + \epsilon_2$, there exist $\epsilon'_1 \in (0, \epsilon_1)$ such that for any positive constant l , $H(l\epsilon_1 + (1-l)\epsilon'_1, \epsilon_2) > H(\epsilon_1, \epsilon_2)$.

□